EUROPEAN ORGANIZATION FOR NUCLEAR RESEARCH (CERN)

CMS-SMP-20-016

Measurement of the electroweak production of Zγ and two jets in proton-proton collisions at $\sqrt{s} = 13$ TeV and constraints on anomalous quartic gauge couplings

The CMS Collaboration*

Abstract

The first observation of the electroweak (EW) production of a Z boson, a photon, and two forward jets (Zγjj) in proton-proton collisions at a center-of-mass energy of 13 TeV is presented. A data set corresponding to an integrated luminosity of 137 fb^{-1}, collected by the CMS experiment at the LHC in 2016–2018 is used. The measured fiducial cross section for EW Zγjj is $\sigma_{EW} = 5.21 \pm 0.52\,\text{(stat)} \pm 0.56\,\text{(syst)}$ fb $= 5.21 \pm 0.76$ fb. Single-differential cross sections in photon, leading lepton, and leading jet transverse momenta, and double-differential cross sections in m_{jj} and $\Delta\eta_{jj}$ are also measured. Exclusion limits on anomalous quartic gauge couplings are derived at 95% confidence level in terms of the effective field theory operators M_0 to M_5, M_7, T_0 to T_2, and T_5 to T_9.

Submitted to Physical Review D

*See Appendix A for the list of collaboration members

arXiv:2106.11082v1 [hep-ex] 21 Jun 2021

1 Introduction

Vector boson scattering (VBS) processes are purely electroweak (EW) interactions at leading order (LO). In a proton-proton (pp) collision where two vector bosons radiated from the incoming quarks scatter, the two outgoing quarks appear as jets widely separated in pseudorapidity (η) and with a large dijet mass (m_{jj}), providing a unique signature. The VBS is of great interest because of the role of the Higgs boson in restoring unitarity to the VBS cross section. Studies of VBS complement direct Higgs boson measurements [1–5] and open a window to beyond the standard model (BSM) scenarios at energy scales outside the reach of direct searches. Standard model (SM) EW production of Z jj, which can proceed through VBS, can be extracted by exploiting the unique features of the VBS signature. A precise measurement of EW Z jj production is sensitive not only to quartic gauge couplings (QGCs) in the SM as well as possible anomalous QGCs (aQGCs) [6], but also to triple gauge couplings (TGCs) and anomalous TGCs. Since the latter is well constrained in diboson production [7], they are not explored in this paper.

In this paper, we present the first observation of EW Z jj production. Events corresponding to the jj final states where e or , are selected, and the dijet system is required to satisfy the typical VBS signature. Fig. 1 shows the representative Feynman diagrams (upper left and center), in which a Z boson and a photon are produced in a scattering interaction between two W bosons, an example of the production of Z jj induced by quantum chromodynamics (upper right), one of the important backgrounds in this study, and examples of non-VBS EW production of Z jj (lower).
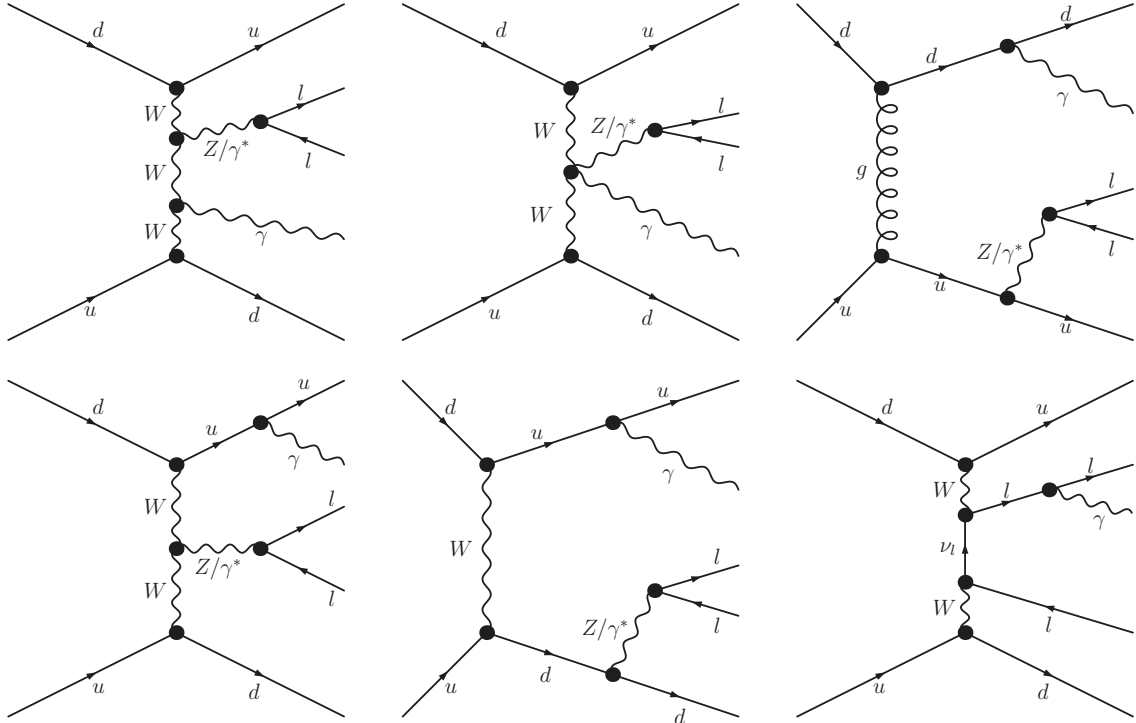

Figure 1: Representative Feynman diagrams for Z jj production. With the exception of the upper right one, the diagrams involve only EW vertices: VBS via W boson (upper left), VBS with QGC (upper center), vector boson fusion with TGCs (lower left), bremsstrahlung (lower center), multiperipheral (lower left), whereas the diagram (upper right) represents a QCD-induced contribution.

Previous experimental results for EW Z jj production have been reported by the ATLAS [8] and CMS [9] Collaborations based on data collected in 2016 at $\sqrt{s}$ 13 TeV, corresponding to integrated luminosities of 35.9 fb^{-1} and 36 fb^{-1}, respectively. The observed (expected) significance reported by ATLAS was 4.1 (4.1) standard deviations (SD), and by CMS was 4.7 (5.5) SD.

The measurements reported here are based on pp collision data at $\sqrt{s}$ 13 TeV, collected from 2016 to 2018 by the CMS experiment at the CERN LHC, corresponding to an integrated luminosity of 137 fb^{-1}. A simultaneous maximum likelihood (ML) fit is used to extract the signal significance, the signal strength, fiducial cross sections, and unfolded differential cross sections for both EW and EW+QCD production of Z jj. Unfolded differential cross sections are measured as functions of three 1-dimensional observables (the transverse momenta (p_T) of the leading lepton, photon, and jet) and one 2-dimensional observable (m_{jj} and $_{jj}$). Using the selected jj events with high photon p_T, constraints on BSM contributions to the VVZ vertices, where V W, Z, or , are determined in an effective field theory (EFT) framework using dimension-8 operators [6].

This paper is arranged as follows. The CMS detector, the data samples, and the event simulation are summarized in Sections 2 and 3. The object reconstruction and the event selection are described in Section 4. The estimation of the main backgrounds is given in Section 5. The systematic uncertainties are discussed in Section 6 and the results are presented in Section 7. The paper is summarized in Section 8.

2 The CMS detector

The central feature of the CMS [10] apparatus is a superconducting solenoid of 6 m internal diameter, providing a magnetic field of 3.8 T. Within the solenoid volume are a silicon pixel and strip tracker, a lead tungstate crystal electromagnetic calorimeter (ECAL), and a brass and scintillator hadron calorimeter (HCAL), each composed of a barrel and two endcap sections. Forward calorimeters extend the coverage provided by the barrel and endcap detectors. Muons are detected in gas-ionization chambers embedded in the steel flux-return yoke outside the solenoid.

Events of interest are selected using a two-level trigger system [11]. The first level (L1), composed of custom hardware processors, uses information from the calorimeters and muon detectors to select events of interest with a maximum rate of 100 kHz within a latency of less than 4 s. The second level is a high-level trigger (HLT) processor, made up of a farm of processors running a version of the full event reconstruction software optimized for fast processing, and decreases the rate to about 1 kHz before storage.

A more detailed description of the CMS detector, together with a definition of the coordinate system and kinematic variables, is reported in Ref. [10].

3 Signal and background simulation

Samples of simulated events are used to model the EW Z jj signal and a variety of background processes. Since the data analyzed for this paper were collected by the CMS experiment from 2016 through 2018, the Monte Carlo (MC) samples are also simulated separately for each year with different versions of the MC generators. The MADGRAPH5_aMC@NLO [12] v2.6.0 (v2.6.1), which is abbreviated as MG5 in the following text, POWHEG [13–16] v2.0, and PYTHIA [17]

v8.226 (v8.230) are used for 2016 (2017 and 2018). The simulated samples are used to establish the event selection, optimize the signal extraction procedure, and estimate the total signal efficiency in the inclusive fiducial volume and single signal efficiency in every bin of final experimental distributions.

The signal EW Z jj production with the Z boson decaying to a pair of leptons is simulated at LO using the MG5 generator. The main backgrounds, including QCD-induced Z (QCD Z) and t$\bar{\text{t}}$ (TT) are generated with MG5 with up to one jet at next-to-leading order (NLO) in QCD using the FxFx jet merging scheme [18]. The remaining backgrounds, including diboson (WW/WZ/ZZ) production (VV) and single top quark production (ST), are generated with either PYTHIA at LO or POWHEG at NLO. The interference between EW Z jj production and QCD-induced Z jj production is also simulated with MG5 at $\mathcal{O}\left(\alpha_{\text{S}}\alpha_{\text{EW}}^{3}\right)$ and treated as a part of QCD-induced Z .

The simulation of aQGCs is performed using MG5 at LO. The matrix element reweighting functionality [19] is employed to produce additional weights that correspond to an appropriately spaced grid for each of the anomalous couplings probed in this paper.

The protons are described in the simulation by the NNPDF 3.0 [20] (NNPDF 3.1 [21]) parton distribution functions (PDFs) for the 2016 (2017 and 2018). The PYTHIA generator package is used for the proton showering, hadronization, and underlying event simulation. The samples are interfaced to PYTHIA with the tune CUETP8M1 (CP5) [22, 23] for the year 2016 (2017 and 2018).

The detector response is modeled via a detailed description of the CMS detector implemented in the GEANT4 package [24, 25]. The simulated events are reconstructed in the same way as the CMS data and include additional interactions in the same and neighboring bunch crossings, referred to as pileup (PU). Simulated PU events are weighted so that the number of reconstructed primary vertices reproduces that observed in the data.

4 Object reconstruction and event selection

4.1 Object reconstruction

The final state of interest consists of a pair of oppositely charged isolated leptons, a photon, and two jets. We employ both a global object reconstruction algorithm and dedicated particle-type (e.g., muon) reconstruction algorithms, for different purposes, as described in the following paragraphs. The global object reconstruction algorithm, called the particle-flow (PF) algorithm [26], reconstructs and identifies all particle candidates (photons, electrons, muons, charged and neutral hadrons, and missing transverse momentum) in an event, based on a combination of information from the various elements of the CMS detector; the result is a set of physics objects called PF candidates.

The candidate vertex with the largest value of summed physics-object p_{T}^{2} is taken to be the primary pp interaction vertex. The physics objects are the jets, clustered using the jet finding algorithm [27, 28] with the tracks assigned to candidate vertices as inputs, and the associated missing transverse momentum, taken as the negative vector sum of the p_{T} of those jets (which include the leptons).

Electron candidates are reconstructed by combining information from the ECAL and the tracker within $|\eta| < 2.5$ and $p_{\text{T}} > 25$ GeV. The energy of electrons is determined from a combination of the electron momentum at the primary interaction vertex determined by the tracker, the energy

of the corresponding ECAL cluster, and the energy sum of all bremsstrahlung photons spatially compatible with originating from the electron track. Reconstructed electrons are required to satisfy additional identification requirements [29] as follows: the relative amount of energy deposited in the HCAL; a matching procedure between the trajectory in the inner tracker and that in the supercluster [30] of the ECAL; the number of missing hits in the inner tracker; the consistency between the track and primary vertex; a shower shape variable $\sigma_{i\eta i\eta}$, which quantifies the transverse spread in η of the electromagnetic shower in the ECAL (discussed in Section 5); and a photon conversion rejection algorithm. An appropriate working point, referred to as the stringent electron selection, which has an average per-electron efficiency of 80%, is used to identify the electron candidates from the Z boson decays in the signal process. A far less restrictive working point, referred to as the minimal electron selection, which has an average per-electron efficiency of 95%, is used to remove events that contain additional electrons.

Muon candidates are reconstructed by combining information from the silicon tracker and the muon system within the region $|\eta| < 2.4$ and $p_T > 20\,\text{GeV}$ [31]. The combined information is used to produce a global track fit, and the muon momenta are obtained from the track curvatures. Muons are selected from the reconstructed muon track candidates by applying additional identification requirements as follows: the number of hits in the muon system and the inner tracker; the quality of the combined fit to a track; the number of matched muon-detector planes; and the consistency between the track and primary vertex. Different muon identification working points are defined according to their efficiency. An appropriate working point, referred to as the stringent muon selection, is used to identify the muon candidates from the Z boson decays in the signal process. The efficiency to reconstruct and identify muons is greater than 96%. A far less restrictive working point, referred to as the minimal muon selection, is used to remove events with additional muons.

Leptons are required to be isolated from other particles in the event. The relative isolation is used and defined as:

$$R_{\text{Iso}} = \left[p_T^{\text{charged}} + \max\left(0, \sum p_T^{\text{neutral}} + \sum p_T^{\gamma} - p_T^{\text{PU}}\right) \right] / p_T, \tag{1}$$

where the sums run over the charged and neutral hadrons, as well as the photons, in a cone of size $\Delta R = \sqrt{\Delta\eta^2 + \Delta\phi^2} < 0.3\ (0.4)$ for the electron (muon) trajectory, where η and ϕ denote the pseudorapidity and azimuthal angle. The quantity p_T^{charged} is the scalar p_T sum of charged hadrons originating from the primary vertex; $\sum p_T^{\text{neutral}}$ and $\sum p_T^{\gamma}$ are the respective scalar p_T sums of neutral hadrons and photons. The contribution from PU in the isolation cone, p_T^{PU}, is subtracted using the FASTJET v3.0.2 technique [28]. For electrons, p_T^{PU} is evaluated using the "jet area" method described in Ref. [32]. For muons, p_T^{PU} is assumed to be half of the scalar p_T sum deposited in the isolation cone by charged particles not associated with the primary vertex. The factor of one half corresponds approximately to the ratio of neutral to charged hadrons produced in the hadronization of PU interactions. Electrons are considered isolated for the stringent (minimal) working points if $R_{\text{Iso}} < 0.0695\ (0.1750)$ in the barrel and $R_{\text{Iso}} < 0.0821\ (0.1590)$ in the endcap detector regions. Muons are considered isolated for the stringent (minimal) working points if $R_{\text{Iso}} < 0.15\ (0.25)$.

The efficiencies of lepton reconstruction and selection are measured as a function of p_T and η for both data events and MC events. The "tag-and-probe" technique [33] is used on events containing a single Z boson. The ratio of efficiencies from events in data and MC are used to correct the simulation. The momentum scales of both muons and electrons are calibrated in bins of p_T and η [29, 34].

Photon reconstruction and selection are similar to electron reconstruction and selection. Pho-

tons located in the barrel region, $|\eta| < 1.442$, and the ECAL endcap region, $1.566 < |\eta| < 2.500$, with $p_\mathrm{T} > 20\,\mathrm{GeV}$, are referred to as γ_barrel and γ_endcap, respectively. The region $1.442 < |\eta| < 1.566$ is a transition region between the barrel and endcaps and is not used for photon reconstruction, because the reconstruction of a photon object in this region is less precise. Reconstructed photons are required to satisfy further quality criteria [29] based on the following quantities: the relative amount of deposited energy in the ECAL and HCAL; isolation variables constructed separately for the charged and neutral hadrons, photons other than the signal photon; and a procedure that quantifies the likelihood for a photon to originate from electron bremsstrahlung. An appropriate working point, referred to as the stringent photon selection, with an average per-photon efficiency of 80%, is used to reconstruct prompt photons (not from hadron decays) in the final state. A second working point, which will be referred to as the nonprompt-enriched photon selection, is used to reconstruct nonprompt photons that are mainly products of neutral pion and η meson decays [29, 35], which constitute an important background in this study.

Jets are reconstructed from particle-flow candidates using the anti-k_T jet clustering algorithm [27], as implemented in the FASTJET package v3.0.2, with a distance parameter of 0.4. The energies of charged hadrons are determined from a combination of their momenta measured in the tracker and the matching of ECAL and HCAL energy deposits, corrected for the response of the calorimeters to hadronic showers. The energy of neutral hadrons is obtained from the corresponding corrected ECAL and HCAL energies. To reduce the instrumental background, as well as the contamination from PU, jets are selected by the stringent jet selection based on the multiplicities and energy fractions carried by charged and neutral hadrons.

Jet energy corrections are extracted from data and simulated events to account for the effects of PU, non-uniformity of the detector response, and residual differences between the jet energy scale (JES) in data and simulation. The JES calibration [36] relies on corrections parameterized in terms of the uncorrected p_T and η of the jet, and is applied as a multiplicative factor, scaling the four-momentum vector of each jet. To ensure that jets are well measured and to reduce the PU contamination, all jets must satisfy $|\eta| < 4.7$ and have a corrected $p_\mathrm{T} > 30\,\mathrm{GeV}$. Jets from PU are further rejected using PU jet identification criteria based on a multivariate technique [37].

4.2 Event selection

The events of interest are selected by dilepton triggers. We denote the lepton having the larger p_T as ℓ_1 and the other one as ℓ_2. The p_T thresholds in the HLT are $p_\mathrm{T}^{\ell_1} > 23\,\mathrm{GeV}$, $p_\mathrm{T}^{\ell_2} > 12\,\mathrm{GeV}$ for electrons, and $p_\mathrm{T}^{\ell_1} > 17\,\mathrm{GeV}$, and $p_\mathrm{T}^{\ell_2} > 8\,\mathrm{GeV}$ for muons. In 2016 and 2017, a timing shift in the ECAL endcap was not properly accounted for in the trigger logic, resulting in the trigger decision sometimes mistakenly being assigned to the previous bunch crossing. This led to a sizable decrease in the L1 trigger efficiency for events with high energy deposits in the ECAL endcaps. The loss of efficiency for EW Z jj events associated with this effect is $\approx 8\%$ for the invariant mass of two jets $m_\mathrm{jj} \approx 500\,\mathrm{GeV}$, and increases to $\approx 15\%$ for $m_\mathrm{jj} \approx 2\,\mathrm{TeV}$. A correction is therefore applied as a function of jet p_T and η using an unbiased data sample with correct timing and is implemented through a factor that represents the probability of the event to avoid having mistimed signals.

Selected events are required to contain two oppositely charged same-flavor leptons, either a pair of electrons or a pair of muons. Both leptons must pass the stringent working points and the corresponding isolation requirements described in Section 4.1 and must satisfy $p_\mathrm{T} > 25$ $(20)\,\mathrm{GeV}$, and $|\eta| < 2.5\ (2.4)$ in the electron (muon) case. The invariant mass of the dilepton system ($m_{\ell\ell}$) is required to be within the window $70 < m_{\ell\ell} < 110\,\mathrm{GeV}$. To reduce the WZ

and ZZ backgrounds, events are rejected that contain any additional lepton passing the less restrictive identification criteria than the one used for electron and muon selection, mentioned in Section 4.1. At least one photon satisfying the stringent identification criteria is required. The photon with the largest p_T in the event is used if there is more than one photon passing the stringent identification criteria. The photon is required to have p_T 20 GeV. The ΔR between the selected photon and each of the selected leptons is required to be larger than 0.7. The invariant mass of the dilepton-photon system must satisfy $m_{\ell\ell\gamma}$ 100 GeV to reduce the contribution from final-state radiation in Z boson decays. The event must also contain at least two jets that satisfy the jet identification criteria described in Section 4.1 and that are separated from selected leptons and photons by ΔR 0.5. The jet with the largest p_T is referred to as the leading jet and is denoted as j1, and the jet with the lower p_T is denoted as j2. The jets are required to satisfy p_T 30 GeV, $|\eta|$ 4.7, and ΔR j1,j2 0.5. The dilepton selection with a photon and two jets is henceforth referred to as the "common" selection.

The signal region is defined by the common selection, and by requiring m_{jj} 500 GeV and $|\Delta\eta_{jj}| = |\eta_{j1} - \eta_{j2}|$ 2.5. Two additional criteria are used for the signal significance measurement. First, the Zeppenfeld variable [38] variable $\eta_Z^* = \eta_Z - (\eta_{j1} + \eta_{j2})/2$, needs to satisfy 2.4. Second, the magnitude of the difference in the azimuthal angle between Zγ and the dijet system, $\Delta\phi_{Z\gamma,jj} = \phi_{Z\gamma} - \phi_{j1j2}$, which should be large in signal events because the two systems are recoiling against each other, must satisfy $\Delta\phi_{Z\gamma,jj}$ 1.9. A low-m_{jj} control region, in which the EW signal is negligible compared with the contribution from QCD-induced Zγjj production, is defined by the common selection and the requirement 150 GeV m_{jj} 500 GeV.

The total and differential cross sections for EW Zγjj and EW+QCD Zγjj production are measured in a fiducial region (see "Fiducial volume" in Table 1) that closely mirrors the EW signal region at the particle level (see "EW signal region" in Table 1). The particle-level leptons and photons are required to be prompt, which means that the photon should be from the VBS process and lepton should be from the Z decay, and the momenta of prompt photons with ΔR 0.1 are added to the lepton momenta to correct for final-state photon radiation.

The selection for the aQGC search is similar to the EW signal selection, but targets the characteristic high-energy behavior of aQGC processes by requiring p_T^γ 120 GeV.

A summary of all the selection criteria is displayed in Table 1.

5 Background estimation

The dominant background arises from the QCD-induced production of Zγjj. The yield and shape of this irreducible background are taken from simulation, but are ultimately constrained by the data in the ML fit mentioned in Section 7.1 that extracts the EW signal. The second most important background arises from events in which the selected photon is not prompt and is mainly from Z+jets events. This background cannot be simulated accurately and is estimated from data, as described in the following paragraph. Other small contributions feature kinematic distributions similar to that of the dominant background and are estimated from simulation including single top quark events in the *s*- and *t*-channels that are normalized to their respective NLO cross sections; associated single top quark and W boson production normalized to its next-to-next-to-leading order (NNLO) cross section [39]; WW production normalized to its NNLO cross section; WZ, ZZ, QCD-induced Wγjj, and $t\bar{t}\gamma$ production normalized to their NLO cross sections.

The background from events containing a nonprompt photon is estimated using data to calcu-

Table 1: Summary of the five sets of event selection criteria used to define events in the fiducial cross section measurement region, control region, EW signal extraction region, and the region used to search for aQGC contributions.

Common selection	$p_T^{1,2} > 25$ GeV, $|\eta^{1,2}| < 2.5$ for electron channel
	$p_T^{1,2} > 20$ GeV, $|\eta^{1,2}| < 2.4$ for muon channel
	$p_T^{\gamma} > 20$ GeV, $|\eta^{\gamma}| < 1.442$ or $1.566 < |\eta^{\gamma}| < 2.500$
	$p_T^{j1,j2} > 30$ GeV, $|\eta^{j1,j2}| < 4.7$
	$70 < m_{\ell\ell} < 110$ GeV, $m_{\ell\ell\gamma} > 100$ GeV
	ΔR_{jj}, $\Delta R_{\ell j}$, $\Delta R_{\gamma j} > 0.5$, $\Delta R_{\ell\gamma} > 0.7$
Fiducial volume	Common selection,
	$m_{jj} > 500$ GeV, $|\Delta\eta_{jj}| > 2.5$
Control region	Common selection,
	$150 < m_{jj} < 500$ GeV
EW signal region	Common selection,
	$m_{jj} > 500$ GeV, $|\Delta\eta_{jj}| > 2.5$,
	$|\eta^{\gamma}| < 2.4$, $|\zeta_{\ell\ell\gamma,jj}| < 1.9$
aQGC search region	Common selection,
	$m_{jj} > 500$ GeV, $|\Delta\eta_{jj}| > 2.5$,
	$p_T^{\gamma} > 120$ GeV

late the event weight of the corresponding nonprompt photon event shown in Eq. (2),

$$ w(p_T) = \frac{n_{\text{data}}(p_T)}{N_{\text{fake}}^{\text{unweighted}}(p_T)} \cdot \text{fake-fraction}(p_T) , \tag{2} $$

in a region similar to our common selection with the jet requirements removed. The numerator n_{data} represents the number of events passing the stringent photon selection. The denominator $N_{\text{fake}}^{\text{unweighted}}$ represents the number of events passing the nonprompt-enriched photon selection mentioned in Section 4.1. The contribution from the signal region is removed for both the numerator and denominator, and the prompt contribution in the denominator is also removed by subtracting the small prompt photon contribution from the data based on simulated samples. The factor fake-fraction is the fraction of nonprompt photons in the region where the stringent photon selection is applied, which is obtained from a template fit of the photon $\sigma_{i\eta i\eta}$ distribution, since the variable $\sigma_{i\eta i\eta}$ quantifies the width of the photon electromagnetic shower in η, which is narrow for prompt and broad for nonprompt photons. The prompt-photon template is obtained from simulated $Z\gamma$ events and the nonprompt-photon template is obtained from a sideband method of inverting the charged hadron isolation variable of the photon in data. The event weight of an event containing a nonprompt photon can be then calculated as a function of p_T for photons in the barrel and endcap regions. The nonprompt-photon background estimate in the signal region is determined by these event weights and the rate of events passing the signal region selection with the stringent photon selection replaced by the nonprompt-enriched photon selection.

6 Systematic uncertainties

The sources of systematic uncertainty can be divided into experimental and theoretical categories. The experimental sources include uncertainties in corrections to the simulation, the method to estimate the nonprompt-photon background contribution, and corrections for detector effects during data taking not properly accounted by the simulation in the experiment. The sources of theoretical uncertainty include the choice of the renormalization and factorization scales, and the choice of the PDFs.

The uncertainty because of renormalization and factorization scales denoted as μ_R and μ_F, respectively, is evaluated for the signal and QCD-induced $Z\gamma jj$ background. The different choices for μ_F and μ_R considered are these six combinations: $(\mu_F, \mu_R) = (2\mu_0, \mu_0), (0.5\mu_0, \mu_0), (\mu_0, 2\mu_0), (\mu_0, 0.5\mu_0), (2\mu_0, 2\mu_0)$, and $(0.5\mu_0, 0.5\mu_0)$, in which μ_0 represents the nominal scale. These six combinations are further divided into three groups according to either μ_R or μ_F not equalling μ_0 or both of them not equalling μ_0. The difference in one group is calculated and regarded as one component of the uncertainties in μ_R and μ_F. The uncertainties of these three components range from 1 to 12% for the EW signal and from 6 to 25% for QCD-induced $Z\gamma jj$ background. All three components are included as independent systematic uncertainties in the ML fit introduced in Section 7.1. The PDF and related strong coupling α_S are evaluated using the eigenvalues of the PDF set following the NNPDF prescription [40]. The size of this uncertainty is 1–3% for both EW signal and QCD-induced $Z\gamma jj$ background.

The uncertainties in the jet modeling, which include the JES, the jet energy resolution (JER), and the PU jet identification, are calculated in simulated events. The JES and JER are obtained by applying the corrections shifted by ± 1 SD. The effect of the updated corrections is propagated to all dependent variables and all selection criteria, and these effects on the yield are determined bin-by-bin for each bin of the m_{jj}-$\Delta\eta_{jj}$ distribution. The variation, $+1$ SD or -1 SD, that has the larger absolute effect on the yield is assumed as the uncertainty. The size of the uncertainty varies between 1 and 92%, depending on the m_{jj}-$\Delta\eta_{jj}$ bin, but the larger values typically correspond to bins where the uncertainty is less important because they are applied to a smaller nominal yield. The uncertainties in PU jet identification are calculated by changing the corresponding scale factors ± 1 SD, depending on p_T and η. The uncertainties in jet energy corrections and PU jet working points are uncorrelated between different years, but correlated between the electron and muon categories.

The systematic uncertainty in the nonprompt-photon background estimate is the quadratic sum of three components. The first component is the uncertainty in the choice of the isolation sideband. The second component is the uncertainty in the bias in the fitting procedure, calculated by performing the procedure in simulated pseudo-data and comparing the fit results with the known fractions. This component, which is larger in the endcap than in the barrel, increases with photon p_T. The third component is the uncertainty in the modeling of the prompt-photon events in the true template fit, estimated as the difference between prompt-photon events simulated from QCD-induced $Z\gamma$ and EW $Z\gamma jj$ signal. The overall uncertainty in the nonprompt-photon background estimation ranges from 9 to 37%, uncorrelated between years and channels.

The uncertainties that arise from the finite number of events in simulated samples and data control regions, referred to as statistical uncertainties, are calculated bin-by-bin based on the Poisson distribution. The statistical uncertainties typically increase with increasing m_{jj} and $\Delta\eta_{jj}$ and are uncorrelated across different processes and bins. The uncertainties in the efficiencies of lepton identification, trigger efficiencies, and photon identification range from 0.5 to 3.0% depending on p_T and η and include both statistical and systematic sources. The systematic

(statistical) uncertainties are dominant in the low (high) p_{T} range.

All simulated samples are also affected by uncertainties associated with the ECAL timing shift, the reweighting of the PU distribution, and the integrated luminosity. The uncertainties associated with the ECAL timing shift correction factors range from 1 to 4%, depending on the process and the m_{jj}-jj bin. The uncertainty from pileup reweighting is evaluated by changing the total inelastic cross section of 69.2 mb [41] by 5%, which results in an uncertainty in the 1–10% range. The integrated luminosity of the 2016, 2017, and 2018 data-taking periods have uncertainties in the 1.2–2.5% range [42–44]. These uncertainties are partially correlated and correspond to a total uncertainty of 1.6%. The uncertainties of ECAL mistiming, reweighting of the PU, and integrated luminosity uncertainties are correlated across years.

All of the above systematic uncertainties are applied in the calculation of the signal significance, measurements of the cross section, and in the search for aQGCs. They are also applied in the cross section measurement, with the exception of the theoretical uncertainties related to the normalization of the signal.

We organize the systematic uncertainties into the following groups: theoretical uncertainties including the scales $_{\mathrm{R}}$ and $_{\mathrm{F}}$, and the PDF uncertainties; corrections applied to jets including JES and JER; uncertainties in the nonprompt-photon background estimate; statistical uncertainties from simulation or data; corrections applied to electron and photon candidates; corrections applied to muon candidates; uncertainties from PU reweighting; uncertainties in the integrated luminosity; uncertainties from the L1 trigger timing shift; and uncertainties from corrections of PU jet identification (ID) working points. The remaining uncertainties, which are referred to as "other", include the uncertainties in the cross section estimation of diboson and $t\bar{t}$ processes that have an impact 0.1%. The uncertainties in $_{\mathrm{R}}$ and $_{\mathrm{F}}$ of the QCD-induced production and in the jet energy correction are the dominant systematic uncertainties in the measurement. The impact of the uncertainty of each group on the signal strength measurement is displayed in Table 2.

Table 2: The impact of the systematic uncertainties on the EW signal strength measurement.

Systematic uncertainty	Impact [%]	
Jet energy correction	+7.9	6.7
Theoretical uncertainties	+5.5	4.7
MC statistical uncertainties	+4.7	4.5
PU	+4.7	4.1
Related to e,	+4.5	3.6
PU jet ID	+3.7	3.4
ECAL timing shift at L1	+3.5	2.8
Nonprompt- bkg. estimate	+2.0	1.6
Related to	+1.7	1.4
Integrated luminosity	+0.8	0.6
Total systematic uncertainty	+14	12

7 Results

The pre-fit (before the simultaneous fit described in Section 7.1) signal and background expected yields, as well as the observed data yields in the signal region, are shown in Figs. 2 and 3 separately for the photon in the ECAL barrel and endcaps, for both the dielectron and dimuon channels.
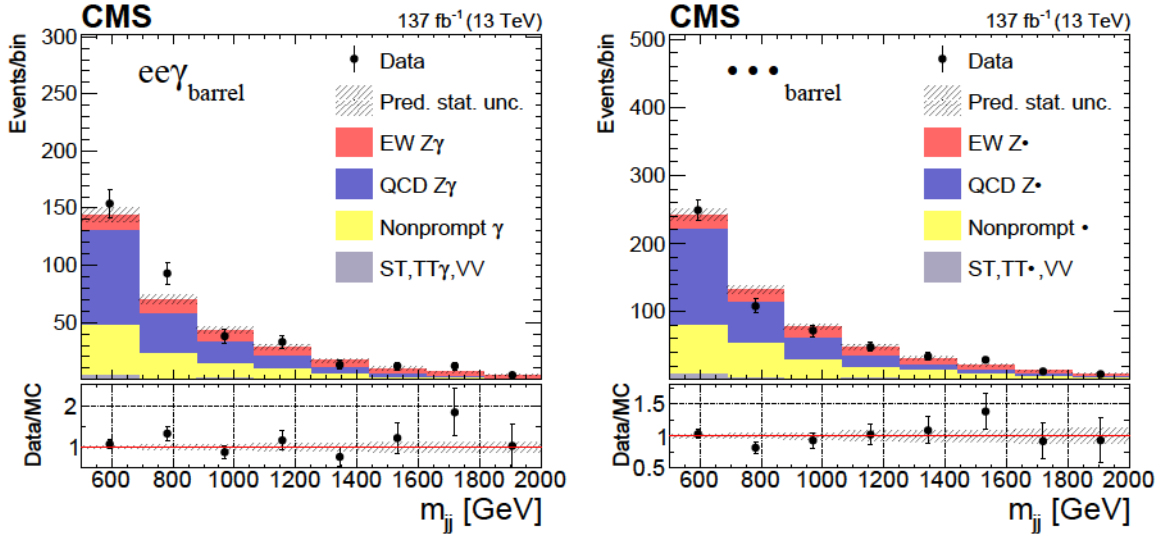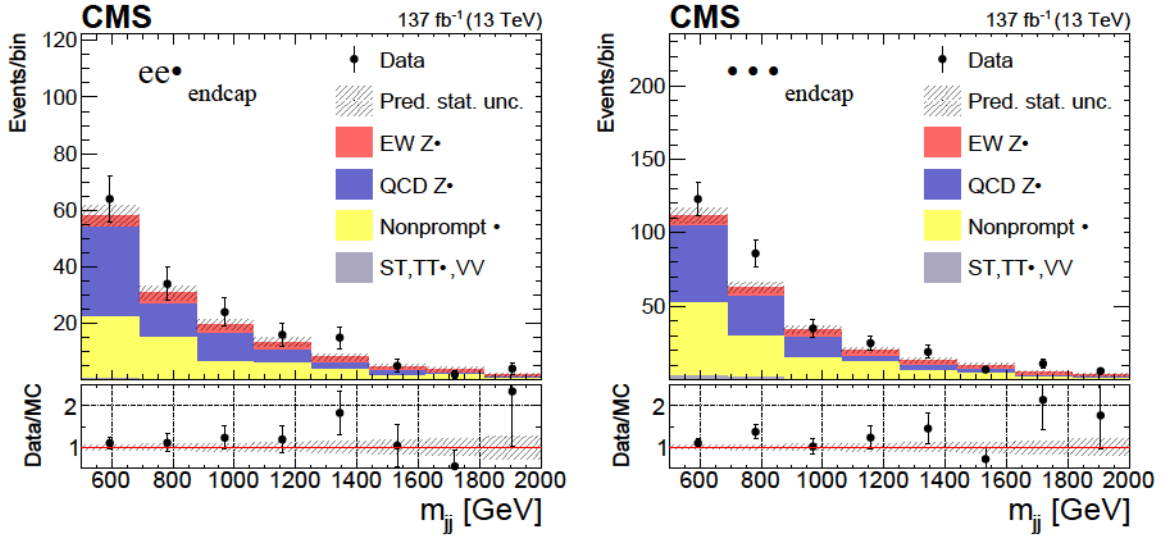
Figure 2: The pre-fit m_{jj} distributions for the dilepton+γ_{barrel} events are shown for the dielectron (left) and the dimuon (right) categories with data collected from 2016 to 2018. The data are compared to the sum of the signal and the background contributions. The black points with error bars represent the data and their statistical uncertainties, whereas the hatched bands represent the statistical uncertainty in the combined signal and background expectations. The last bin includes overflow events. The lower panel shows the ratio of the data to the expectation.

Figure 3: The pre-fit m_{jj} distributions for the dilepton+γ_{endcap} events are shown for the dielectron (left) and the dimuon (right) categories with data collected from 2016 to 2018. The data are compared to the sum of the signal and the background contributions. The black points with error bars represent the data and their statistical uncertainties, whereas the hatched bands represent the statistical uncertainty in the combined signal and background expectations. The last bin includes overflow events. The lower panel shows the ratio of the data to the expectation.

7.1 Measurement of the signal significance

To extract as much information as possible from the data set, we perform a likelihood-based statistical analysis. An optimal binning leads to the best expected signal significance used. The likelihood function is the product of the binned signal and backgrounds probability density functions (pdf), which are expected to follow the Poisson distribution:

$$\mathcal{L} \prod_i^N \text{Poisson}\left(n_i \mid s_j + b_j, p(\tilde{\theta})\right), \tag{3}$$

where n_i is the number of observed events in data, s_i and b_i are the expected event yields for the signal and backgrounds, N represents the number of bins in the signal and control regions, and $p(\tilde{\theta})$ is a Gaussian constrained pdf of the effects of the systematic uncertainties called nuisance parameters (NP), in which $\tilde{\theta}$ represents the external measurements corresponding to each NP. The parameter of interest (POI) μ is the signal strength, which represents the ratio of observed to expected signal yields. The POI μ is estimated by maximizing the profile likelihood ratio defined as:

$$\frac{\mathcal{L}\left(\mu, \hat{\hat{\theta}}\right)}{\mathcal{L}\left(\hat{\mu}, \hat{\theta}\right)}. \tag{4}$$

The numerator of this ratio is the profile likelihood function. The quantity $\hat{\hat{\theta}}$ denotes the value of θ that maximizes $\mathcal{L}$ for the specified μ; it is the conditional ML estimator of θ (and thus is a function of μ). The denominator is the maximized (unconditional) likelihood function, $\hat{\mu}$ and $\hat{\theta}$ are their ML estimators. The presence of the nuisance parameters broadens the profile likelihood as a function of μ relative to that if their values were fixed. This reflects the loss of information about μ because of the systematic uncertainties. If $\mu = 0$, there are no signal events, corresponding to the background-only hypothesis. A test statistic is defined as t $-2\ln\lambda$. Higher values of t thus correspond to increasing incompatibility between the data and the background-only hypothesis. To quantify the level of disagreement between the data and the background-only hypothesis, the p-value [45] is computed using Eq. (5), where t_0 $-2\ln\mathcal{L}\left(0, \hat{\hat{\theta}}_0\right)/\mathcal{L}\left(\hat{\mu}, \hat{\theta}\right)$ and $f(t_0 \mid 0)$ denotes the probability density function of the statistic t_0 under assumption of the background-only ($\mu = 0$) hypothesis [46].

$$p_0 \int_{t_{0,obs}} f(t_0 \mid 0)\, \mathrm{d}t_0. \tag{5}$$

The p-value is then converted to a significance based on the area in the tail of a normal distribution.

The control and signal regions are each divided separately for photons in the ECAL barrel/endcaps and for the dielectron and dimuon channels. The signal region is divided further into bins in m_{jj} and $\Delta\eta_{jj}$, as shown in Figs. 4 and 5. The control region is divided into bins in m_{jj}, as shown in Figs. 6 and 7. The postfit yields for every process and for data are listed in Table 3.

The main contributions to the significance are from the bins in the signal region with an excess of signal relative to background events, such as high m_{jj} bins in each channel.

The observed (expected) significance for EW signal obtained from a simultaneous fit of all bins in the signal region and the control region to the data (Asimov data set [46]) is 9.4 (8.5 SD).

Table 3: Post-fit yields of predicted signal and background with total uncertainties, and observed event counts after the selection in the EW signal region. The γ_{barrel} and γ_{endcap} columns represent events with photons in the ECAL barrel and endcaps, respectively.

Process	$\mu\mu\gamma_{\text{barrel}}$	$\mu\mu\gamma_{\text{endcap}}$	$ee\gamma_{\text{barrel}}$	$ee\gamma_{\text{endcap}}$
ST	0.7 ± 0.4	0.2 ± 0.2	0.6 ± 0.3	0.2 ± 0.2
TTγ	8.8 ± 1.3	2.1 ± 0.5	3.4 ± 0.6	0.2 ± 0.2
VV	6.0 ± 1.9	3.2 ± 1.2	4.1 ± 1.3	0.8 ± 0.3
Nonprompt photon	189 ± 9.2	143 ± 6.9	93.6 ± 6.5	74.3 ± 5.0
QCD $Z\gamma$	274 ± 10	108 ± 5.6	162 ± 7.4	62.4 ± 3.9
EW $Z\gamma$	133 ± 4.7	46.5 ± 1.7	84.5 ± 3.1	28.2 ± 1.1
Predicted yields	612 ± 13	303 ± 8	349 ± 9	166 ± 6
Data	584	320	375	174
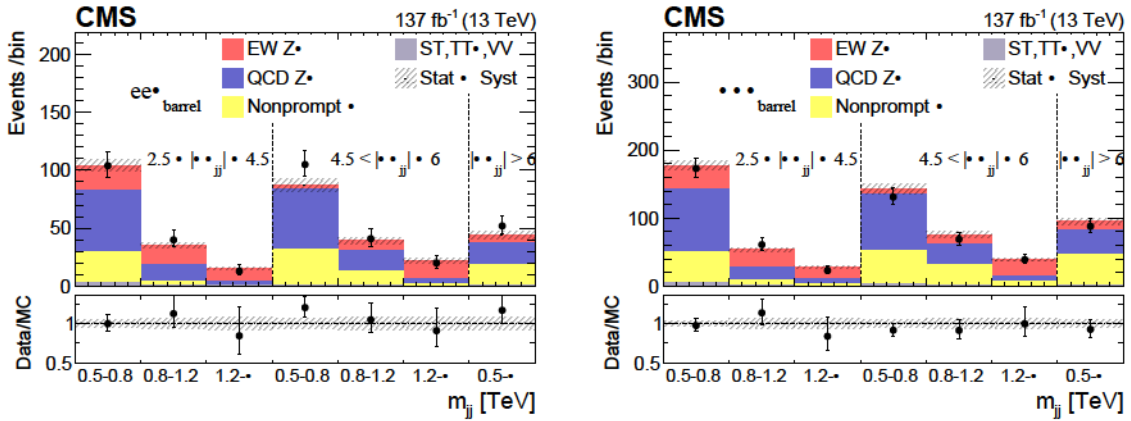
Figure 4: The post-fit 2D distributions of the dielectron (left) and dimuon (right) for the γ_{barrel} categories, as functions of m_{jj} in bins of $|\Delta\eta_{jj}|$. The horizontal axis is split into bins of $|\Delta\eta_{jj}|$ of [2.5, 4.5], [4.5, 6.0], and >6.0. The data are compared to the signal and background in the predictions. The black points with error bars represent the data and their statistical uncertainties, whereas the hatched bands represent the total uncertainties of the predictions.
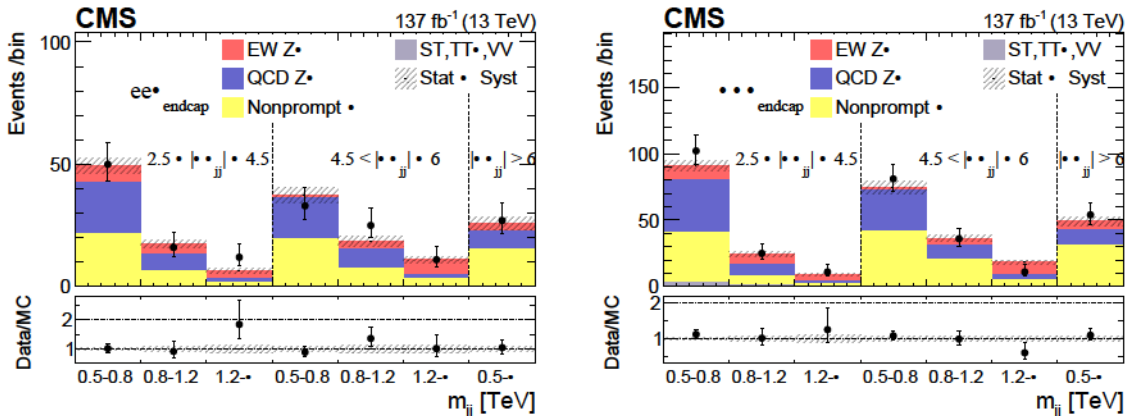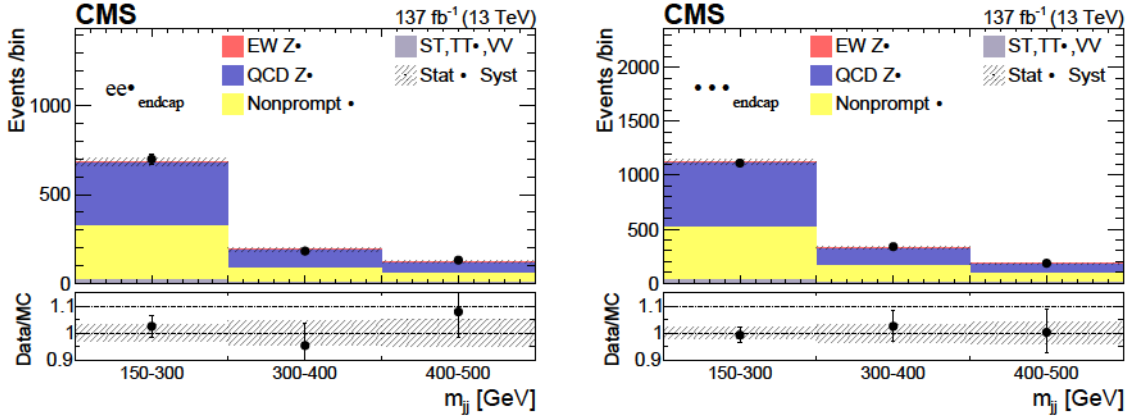

Figure 5: The post-fit 2D distributions of the dielectron (left) and dimuon (right) for the γ_{endcap} categories, as functions of m_{jj} in bins of $|\Delta\eta_{jj}|$. The horizontal axis is split into bins of $|\Delta\eta_{jj}|$ of [2.5, 4.5], [4.5, 6.0], and >6.0. The data are compared to the signal and background in the predictions. The black points with error bars represent the data and their statistical uncertainties, whereas the hatched bands represent the total uncertainties of the predictions.
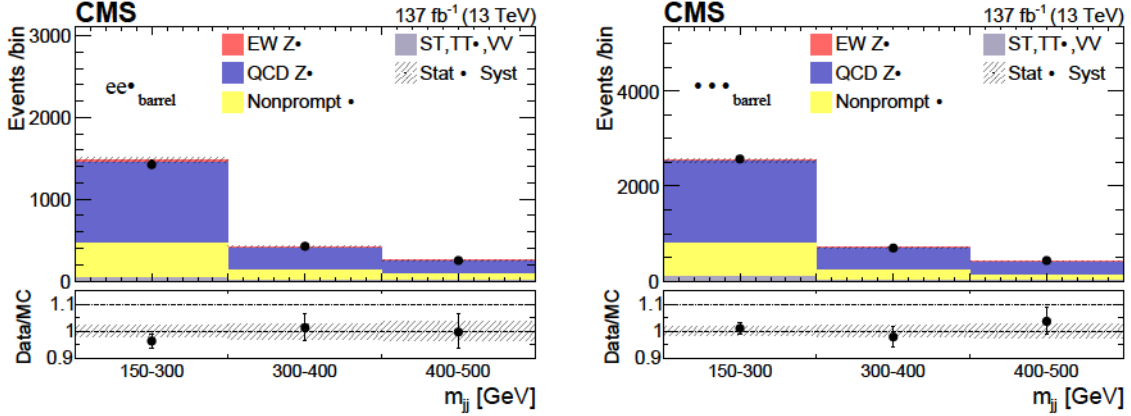
Figure 6: The post-fit distributions in the control region for the dielectron (left) and dimuon (right) for the γ_{barrel} categories as a function of m_{jj}. The horizontal axis is split into bins of m_{jj} of [150, 300], [300, 400], and [400,500]. The black points with error bars represent the data and their statistical uncertainties, whereas the hatched bands represent the total uncertainties of the predictions.

Figure 7: The post-fit distributions in the control region for the dielectron (left) and dimuon (right) for the γ_{endcap} categories as a function of m_{jj}. The horizontal axis is split into bins of m_{jj} of [150, 300], [300, 400], and [400,500]. The black points with error bars represent the data and their statistical uncertainties, whereas the hatched bands represent the total uncertainties of the predictions.

7.2 Fiducial cross section

Fiducial cross sections are measured in the fiducial region, which is designed to mirror the signal region as closely as possible, as shown in Table 1. The fiducial cross section is extracted using the same binning of m_{jj} and $|\Delta\eta_{jj}|$ as used in the signal significance measurement, and with the same simultaneous fit in all regions and channels, with the following exception: the events that pass the EW signal selection but fail the fiducial selection are regarded as a background. We define the fiducial cross section as:

$$\sigma^{fid} = \sigma^g \hat{\mu} a^{gf}, \qquad (6)$$

where σ^g is the cross section for the generated signal events, $\hat{\mu}$ is the signal strength parameter, and a^{gf} is the acceptance for the events generated in the fiducial region and evaluated through simulation. The theoretical fiducial cross section for the EW $Z\gamma$ signal at LO accuracy is 4.34 ± 0.26 (scale) ± 0.06 (PDF) fb. The best fit value for the EW $Z\gamma$ signal strength and the measured

14

fiducial cross section are

$$\mu_{\text{EW}} = 1.20 \, {}^{+0.12}_{-0.12}\,(\text{stat}) \, {}^{+0.14}_{-0.12}\,(\text{syst})$$
$$= 1.20 \, {}^{+0.18}_{-0.17}, \tag{7a}$$

$$\sigma^{\text{fid}}_{\text{EW}} = 5.21 \pm 0.52\,(\text{stat}) \pm 0.56\,(\text{syst})\ \text{fb}$$
$$= 5.21 \pm 0.76\ \text{fb}. \tag{7b}$$

A combined EW+QCD Z jj cross section is also measured in the same fiducial region using the same procedure, except that the control region is excluded. In this measurement, both the EW and QCD contributions are considered signal. The combined Z jj cross section is defined as

$$\sigma^{\text{fid}} = \mu^{\text{g}}_{\text{EW}} a^{\text{gf}}_{\text{EW}} + \mu^{\text{g}}_{\text{QCD}} a^{\text{gf}}_{\text{QCD}}. \tag{8}$$

The theoretical fiducial cross section for QCD Z jj production is $8.93 \pm 1.70\,(\text{scale}) \pm 0.08\ \text{PDF}$ fb. The expected fiducial cross section for the combined QCD and EW Z jj production is $13.3 \pm 1.72\,(\text{scale}) \pm 0.10\ \text{PDF}$ fb. The best fit value for the combined Z jj signal strength and the measured cross section are

$$\mu_{\text{EW}+\text{QCD}} = 1.11 \, {}^{+0.06}_{-0.06}\,(\text{stat}) \, {}^{+0.10}_{-0.09}\,(\text{syst})$$
$$= 1.11 \, {}^{+0.12}_{-0.11}, \tag{9a}$$

$$\sigma^{\text{fid}}_{\text{EW}+\text{QCD}} = 14.7 \pm 0.80\,(\text{stat}) \pm 1.26\,(\text{syst})\ \text{fb}$$
$$= 14.7 \pm 1.53\ \text{fb}. \tag{9b}$$

7.3 Unfolded differential cross section distribution

Unfolding is used to correct measured detector-level distributions to the particle-level by accounting for the limited acceptance, the finite resolution, and inefficiencies of the detector for bin-to-bin migration between the measured and corrected distribution. Simulated EW samples from MC event generators are used to perform the unfolding. Distributions obtained from the generated events correspond to the particle level (which will be referred to as "gen"). The same distributions obtained using simulated events correspond to detector level (which will be referred to as "reco"). In the well-defined fiducial phase space, the events in "reco" and "gen" follow the relation:

$$y_i^{\text{reco}} = \sum_j R_{ij} x_j^{\text{gen}} + b_i, \tag{10a}$$

$$R_{ij} = P(\text{observed in bin } i \mid \text{generated in bin } j), \tag{10b}$$

in which y_i^{reco} represents observed events in data in the reconstructed bin i, x_j^{gen} represents the events from simulation in the bin j at the particle level, and b_i represents the background from simulation in the reconstructed bin i. The number of events $\sum_j x_j^{\text{gen}}$ obeys the distribution $x \sim \text{Poisson}(\mu)$, where μ represents the bin means of the distributions at the particle level. So the observed number of events $\sum_i y_i^{\text{reco}}$ is Poisson distributed, $y \sim \text{Poisson}(\mathbf{R}\mu + b)$, where the element of the response matrix $\mathbf{R}$ is given in the Eq. (10b). The formal solution to Eq. (10a) can be written as $x_j^{\text{gen}} = \sum R_{ji}^{-1}(y_i^{\text{reco}} - b_i)$. The estimate of the x_j^{gen} can also be derived from the principle of ML; the corresponding likelihood is in Eq. (11).

$$\mathcal{L} = \prod_i \text{Poisson}\left(y_i; \sum_j R_{ij}\mu_j s_j + b_i\right) p(\tilde{\theta}). \tag{11}$$

This solution is based on the assumption that R is nonsingular and insensitive to small perturbations. If that is not the case, the problem is ill-posed and R is ill-conditioned, which means that a regularization [47] method is needed. The sensitivity to fluctuations associated with the ML solution can be quantified by the condition number of R, which is a measure of how ill-conditioned the problem is. In general, if the condition number $c(R)$ is small (less than 10), then the problem can most likely be solved using the unregularized ML estimate. In this paper, an appropriate choice of binning is made to guarantee that the response matrix R is nonsingular and $c(R) < 10$. The regularization parts thus are not considered in this unfolded differential cross section measurement.

The unfolded differential cross section is measured in the same way as the fiducial cross section, with a simultaneous fit to data in the control region and signal region in bins of the single variables leading photon p_T, leading lepton p_T, and leading jet p_T, and in bins of two variables m_{jj} and $|\Delta\eta_{jj}|$. The off-diagonal elements of the response matrix correspond to 1% for leading photon p_T, 1% for leading lepton p_T, 3% for leading jet p_T, and around 5% for m_{jj} and $|\Delta\eta_{jj}|$. All systematic uncertainties discussed in Section 6 are also considered for the corresponding process, especially for the the evaluation of R_{ij}. The signal strengths for each bin of the EW $Z\gamma jj$ unfolded distribution are listed in Tables 4 and 5 and the corresponding differential cross section distributions are shown in Fig. 8.
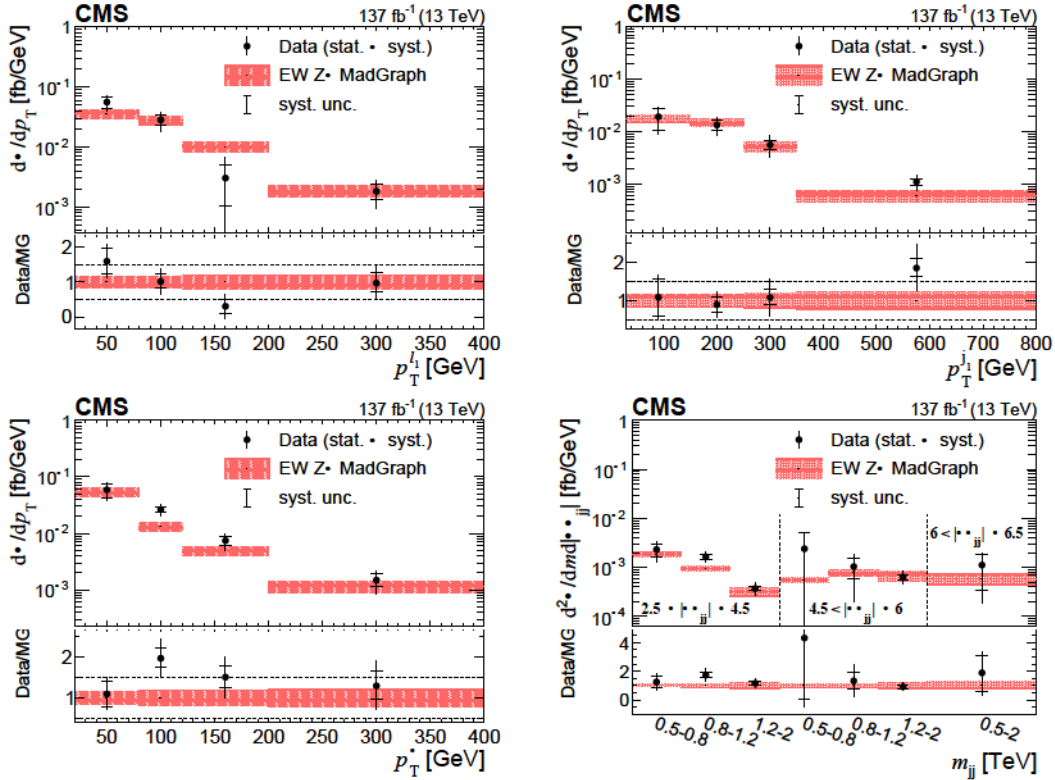
Figure 8: Unfolded differential cross section as a function of the leading lepton p_T, leading jet p_T, leading photon p_T, and m_{jj}-$|\Delta\eta_{jj}|$ for EW $Z\gamma jj$. The black points with error bars represent the data and their statistical uncertainties, whereas the red bands represent the total theoretical uncertainties from the MG5 simulation. The last bin includes overflow events.

A combined EW+QCD $Z\gamma jj$ unfolded differential cross section is also measured in the same region using the same procedure, except that the control region is excluded. In this measurement, both the EW and QCD contributions are considered signal. The combined $Z\gamma jj$ unfolded

Table 4: The signal strengths and differential cross sections from SM expectation and fit calculated as part of the unfolding of p_T, $p_\mathrm{T}^{\mathrm{j_1}}$, and $p_\mathrm{T}^{\ell_1}$ observables for EW Z jj. The last bin includes overflow events.

Variables	Bin [GeV]		Predicted dσ/dp_T [fb/GeV]		Observed dσ/dp_T [fb/GeV]	
$p_\mathrm{T}^{\ell\ell}$	20–80	$1.10^{0.39}_{0.38}$	0.0539	0.0089	0.059	0.021
	80–120	$1.96^{0.46}_{0.43}$	0.0134	0.0024	0.0264	0.0060
	120–200	$1.51^{0.50}_{0.46}$	0.0049	0.0010	0.0074	0.0024
	200–400	$1.29^{0.63}_{0.57}$	0.00114	0.00025	0.00147	0.00068
$p_\mathrm{T}^{\mathrm{j_1}}$	30–150	$1.09^{0.59}_{0.58}$	0.0176	0.0028	0.019	0.010
	150–250	$0.89^{0.34}_{0.33}$	0.0149	0.0026	0.0133	0.0050
	250–350	$1.08^{0.50}_{0.47}$	0.0052	0.0010	0.0056	0.0025
	350–800	$1.86^{0.63}_{0.57}$	0.00059	0.00014	0.00109	0.0036
$p_\mathrm{T}^{\ell_1}$	20–80	$1.60^{0.47}_{0.47}$	0.0350	0.0055	0.056	0.016
	80–120	$1.01^{0.37}_{0.35}$	0.0278	0.0048	0.028	0.010
	120–200	$0.30^{0.36}_{0.34}$	0.0100	0.0019	0.0030	0.00035
	200–400	$0.97^{0.52}_{0.47}$	0.00187	0.00041	0.00188	0.00092

Table 5: The signal strengths and differential cross sections from SM expectation and fit calculated as part of the unfolding of 2D m_{jj}-$\Delta\phi_{\mathrm{jj}}$ observables for EW Z jj. The last bin includes overflow events.

$\Delta\phi_{\mathrm{jj}}$ bin	m_{jj} bin [GeV]		Predicted d$^2\sigma$/dmd$\Delta\phi_{\mathrm{jj}}$ [fb/GeV]		Observed d$^2\sigma$/dmd$\Delta\phi_{\mathrm{jj}}$ [fb/GeV]	
[2.5, 4.5)	[500, 800)	$1.25^{0.59}_{0.58}$	0.00185	0.00017	0.0023	0.0011
[2.5, 4.5)	[800, 1200)	$1.73^{0.43}_{0.40}$	0.00096	0.00014	0.00166	0.00040
[2.5, 4.5)	[1200, 2000]	$1.16^{0.34}_{0.30}$	0.000322	0.000065	0.00037	0.00011
[4.5, 6.0)	[500, 800)	$4.3^{5.1}_{4.8}$	0.000559	0.000057	0.0024	0.0028
[4.5, 6.0)	[800, 1200)	$1.3^{1.1}_{1.1}$	0.00078	0.00012	0.00104	0.00086
[4.5, 6.0)	[1200, 2000]	$0.92^{0.28}_{0.26}$	0.00069	0.00016	0.00064	0.00019
[6.0, 6.5]	[500, 2000]	$1.9^{1.5}_{1.6}$	0.00060	0.00016	0.00112	0.00092

differential cross section is shown in Fig. 9, and Tables 6 and 7. Within the uncertainties, the unfolded distributions agree well with the SM predictions.

7.4 Limits on anomalous quartic gauge couplings

In an EFT approach to BSM physics, dimension-8 operators are constructed from contractions of the covariant derivative of the Higgs doublet and the charged and neutral field strength tensors associated with gauge bosons. Assuming the $SU(2) \times U(1)$ symmetry of the EW gauge field, nine independent charge-conjugate and parity-conserving dimension-8 operators are constructed [6]. The operators affecting the Z jj channel can be divided into those containing an $SU(2)$ field strength, the $U(1)$ field strength, and the covariant derivative of the Higgs doublet, $\mathcal{L}_{\mathrm{M}_{0-5,7}}$, and those containing only the two field strengths, $\mathcal{L}_{\mathrm{T}_{0-2,5-9}}$. The coefficient of the operator $\mathcal{L}_{\mathrm{X_Y}}$ is denoted by $F_{\mathrm{XY}}/\Lambda^4$, where Λ is the unknown scale of BSM physics.

The effects of the aQGCs in addition to the SM EW Z process, as well as interference between the EW and QCD-induced processes, are simulated as described in Section 3. The contribution from aQGCs enhances the production of events at large Z mass, so the m_{Z} distribution is
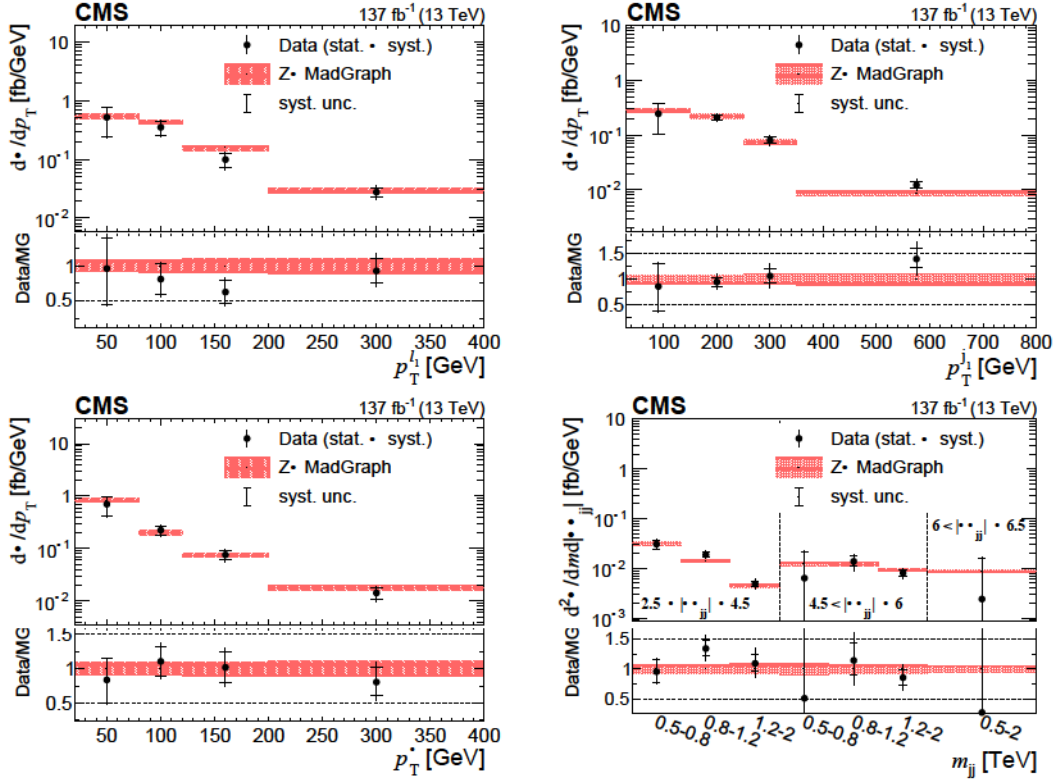
Figure 9: Unfolded differential cross section as a function of the leading lepton p_T, leading photon p_T, leading jet p_T, and m_{jj}-$|\Delta\eta_{jj}|$ for EW+QCD $Z\gamma jj$. The black points with error bars represent the data and their statistical uncertainties, whereas the red bands represent the total theoretical uncertainties from the MG5 simulation. The last bin includes overflow events.

Table 6: The signal strengths and differential cross sections from SM expectation and fit calculated as part of the unfolding of p_T^γ, $p_T^{j_1}$, and $p_T^{\ell_1}$ observables for EW+QCD $Z\gamma jj$. The last bin includes overflow events.

Variables	Bin [GeV]	$\mu \pm \Delta\mu$	Predicted $d\sigma/dp_T$ [fb/GeV]	Observed $d\sigma/dp_T$ [fb/GeV]
p_T^γ	20–80	$0.84^{+0.32}_{-0.35}$	0.841 ± 0.075	0.70 ± 0.029
	80–120	$1.11^{+0.27}_{-0.26}$	0.203 ± 0.019	0.225 ± 0.053
	120–200	$1.02^{+0.29}_{-0.27}$	0.0747 ± 0.0076	0.076 ± 0.022
	200–400	$0.81^{+0.29}_{-0.26}$	0.0176 ± 0.0021	0.0142 ± 0.0049
$p_T^{j_1}$	30–150	$0.86^{+0.46}_{-0.50}$	0.286 ± 0.025	0.25 ± 0.14
	150–250	$0.95^{+0.15}_{-0.14}$	0.222 ± 0.020	0.210 ± 0.032
	250–350	$1.06^{+0.25}_{-0.23}$	0.0759 ± 0.0077	0.081 ± 0.019
	350–800	$1.40^{+0.35}_{-0.31}$	0.0087 ± 0.0010	0.0123 ± 0.0029
$p_T^{\ell_1}$	20–80	$0.96^{+0.45}_{-0.53}$	0.538 ± 0.046	0.52 ± 0.26
	80–120	$0.81^{+0.24}_{-0.25}$	0.431 ± 0.040	0.35 ± 0.11
	120–200	$0.63^{+0.20}_{-0.20}$	0.158 ± 0.016	0.099 ± 0.032
	200–400	$0.93^{+0.26}_{-0.23}$	0.0297 ± 0.0034	0.0276 ± 0.0072

Table 7: The signal strengths and differential cross sections from SM expectation and fit calculated as part of the unfolding of 2D m_{jj}-$|\Delta\eta_{jj}|$ observables for EW+QCD $Z\gamma jj$. The last bin includes overflow events.

$|\Delta\eta_{jj}|$ bin	m_{jj} bin [GeV]	$\mu \pm \Delta\mu$	Predicted $d^2\sigma/dm\,d|\Delta\eta_{jj}|$ [fb/GeV]	Observed $d^2\sigma/dm\,d|\Delta\eta_{jj}|$ [fb/GeV]
[2.5, 4.5)	[500, 800)	$0.96^{+0.23}_{-0.21}$	0.0319 ± 0.0023	0.0306 ± 0.0070
[2.5, 4.5)	[800, 1200)	$1.34^{+0.23}_{-0.21}$	0.0140 ± 0.0011	0.0189 ± 0.0031
[2.5, 4.5)	[1200, 2000]	$1.09^{+0.26}_{-0.23}$	0.00445 ± 0.00038	0.0049 ± 0.0010
[4.5, 6.0)	[500, 800)	$0.52^{+1.3}_{-1.3}$	0.0123 ± 0.0012	0.006 ± 0.016
[4.5, 6.0)	[800, 1200)	$1.14^{+0.46}_{-0.42}$	0.0121 ± 0.0010	0.0138 ± 0.0053
[4.5, 6.0)	[1200, 2000]	$0.86^{+0.22}_{-0.20}$	0.00942 ± 0.00076	0.0081 ± 0.0020
[6.0, 6.5]	[500, 2000]	$0.3^{+1.6}_{-1.6}$	0.00864 ± 0.00049	0.0024 ± 0.0014

used to extract limits on the aQGC parameters. To obtain the prediction for the signal as a function of the value of the aQGC parameter, a quadratic function is used to fit the ratio of aQGC and SM yields in each bin of $m_{Z\gamma}$ in the aQGC region defined in Section 4.2. From Fig. 10, no statistically significant excess of events relative to the SM prediction is observed.
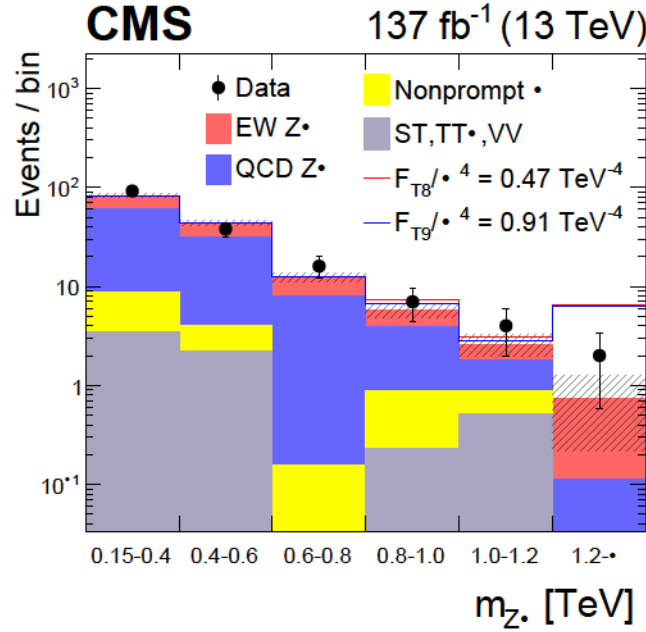
Figure 10: The $m_{Z\gamma}$ distribution for events satisfying the aQGC region selection, which is used to set constraints on the anomalous coupling parameters. The bins of $m_{Z\gamma}$ are [150, 400, 600, 800, 1000, 1200, 2000] GeV, where the last bin includes overflow events. The red line represents a nonzero F_{T8} value and the blue line represents a nonzero F_{T9} value, which would significantly enhance the yields at high $m_{Z\gamma}$. The black points with error bars represent the data and their statistical uncertainties, whereas the hatched bands represent the statistical uncertainties in the SM predictions.

The likelihood function is the product of Poisson distributions and a normal constraining term with nuisance parameters representing the sources of systematic uncertainties in any given bin. The final likelihood function is the product of the likelihood functions of the electron and muon

channels. This test statistic,

$$t_{\text{test}} = -2\ln\frac{\mathcal{L}_{\text{test},\hat{\hat{\theta}}}}{\mathcal{L}_{\hat{},\hat{\theta}}}, \tag{12}$$

is essentially the same test statistic as in Section 7.1 except that the $_{\text{test}}$ represents the aQGC point being tested. The symbol θ represents a vector of nuisance parameters assumed to follow log-normal distributions. The parameter $\hat{\hat{\theta}}$ corresponds to the maximum of the likelihood function at the point $_{\text{test}}$. The $\hat{}$ and $\hat{\theta}$ parameters correspond to the global maximum of the likelihood function.

This test statistic is assumed to follow a χ^2 distribution [48]. It is therefore possible to extract the limits immediately from twice the difference in the log-likelihood function $2\,\Delta\text{NLL} = t_{\text{test}}$ [49]. The observed and expected 95% confidence level limits for the coefficients, shown in Table 8, are obtained by varying the coefficients of one operator at a time and setting all other anomalous couplings to zero. The statistical uncertainties is dominant in the limits setting. The unitarity bound is defined as the scattering energy at which the aQGC coupling strength is set equal to the observed limit that would result in a scattering amplitude that violates unitarity [50]. These results provide the most stringent limit to date on the aQGC parameters F_{T9}/Λ^4.

Table 8: The expected and observed limits on the aQGC parameters at 95% confidence level. The last column presents the scattering energy values for which the amplitude would violate unitarity for the observed value of the aQGC parameter. All coupling parameter limits are set in TeV^{-4}, whereas the unitarity bounds are in TeV.

Coupling	Exp. lower	Exp. upper	Obs. lower	Obs. upper	Unitarity bound
F_{M0}/Λ^4	12.5	12.8	15.8	16.0	1.3
F_{M1}/Λ^4	28.1	27.0	35.0	34.7	1.5
F_{M2}/Λ^4	5.21	5.12	6.55	6.49	1.5
F_{M3}/Λ^4	10.2	10.3	13.0	13.0	1.8
F_{M4}/Λ^4	10.2	10.2	13.0	12.7	1.7
F_{M5}/Λ^4	17.6	16.8	22.2	21.3	1.7
F_{M7}/Λ^4	44.7	45.0	56.6	55.9	1.6
F_{T0}/Λ^4	0.52	0.44	0.64	0.57	1.9
F_{T1}/Λ^4	0.65	0.63	0.81	0.90	2.0
F_{T2}/Λ^4	1.36	1.21	1.68	1.54	1.9
F_{T5}/Λ^4	0.45	0.52	0.58	0.64	2.2
F_{T6}/Λ^4	1.02	1.07	1.30	1.33	2.0
F_{T7}/Λ^4	1.67	1.97	2.15	2.43	2.2
F_{T8}/Λ^4	0.36	0.36	0.47	0.47	1.8
F_{T9}/Λ^4	0.72	0.72	0.91	0.91	1.9

8 Summary

This paper presents the first observation of the electroweak (EW) production of a Z boson, a photon, and two jets (Zγjj) in $\sqrt{s} = 13\,\text{TeV}$ proton-proton collisions recorded with the CMS detector in 2016–2018 corresponding to an integrated luminosity of 137 fb^{-1}. Events were selected by requiring two opposite-sign leptons with the same flavor from the decay of a Z boson, one identified photon, and two jets that have a large separation in pseudorapidity and a large dijet mass. The measured cross section in the fiducial volume defined in Table 1 for EW Zγjj

production is $5.21 \pm 0.52\,\text{(stat)} \pm 0.56\,\text{(syst)}\,\text{fb} \pm 5.21 \pm 0.76\,\text{fb}$, and the fiducial cross section of EW and QCD-induced production is $14.7 \pm 0.80\,\text{(stat)} \pm 1.26\,\text{(syst)}\,\text{fb} \pm 14.7 \pm 1.53\,\text{fb}$. Both the observed and expected signal significances are well in excess of 5 standard deviations. Differential cross sections for EW and EW+QCD are measured for several observables and compared to standard model predictions computed at leading order. Within the uncertainties, the measurements agree with the predictions. Constraints are set on the effective field theory dimension-8 operators M_0 to M_5, M_7, T_0 to T_2, and T_5 to T_9, giving rise to anomalous quartic gauge couplings. These constraints are either competitive with or more stringent than those previously obtained.

Acknowledgments

References

[1] ATLAS Collaboration, "Observation of a new particle in the search for the standard model Higgs boson with the ATLAS detector at the LHC", *Phys. Lett. B* **716** (2012) 1, `doi:10.1016/j.physletb.2012.08.020`, `arXiv:1207.7214`.

[2] CMS Collaboration, "Observation of a new boson at a mass of 125 GeV with the CMS experiment at the LHC", *Phys. Lett. B* **716** (2012) 30, `doi:10.1016/j.physletb.2012.08.021`, `arXiv:1207.7235`.

[3] CMS Collaboration, "Observation of a new boson with mass near 125 GeV in pp collisions at $\sqrt{s}$ 7 and 8 TeV", *JHEP* **06** (2013) 081, `doi:10.1007/JHEP06(2013)081`, `arXiv:1303.4571`.

[4] ATLAS, CMS Collaboration, "Measurements of the Higgs boson production and decay rates and constraints on its couplings from a combined ATLAS and CMS analysis of the LHC pp collision data at $\sqrt{s}$ 7 and 8 TeV", *JHEP* **08** (2016) 045, `doi:10.1007/JHEP08(2016)045`, `arXiv:1606.02266`.

[5] CMS Collaboration, "Combined measurements of Higgs boson couplings in proton-proton collisions at $\sqrt{s}$ 13 TeV", *Eur. Phys. J. C* **79** (2019) 421, `doi:10.1140/epjc/s10052-019-6909-y`, `arXiv:1809.10733`.

[6] O. J. P. Éboli, M. C. Gonzalez-Garcia, and J. K. Mizukoshi, "pp jje and jje at $\mathcal{O}(\alpha_{em}^6)$ and $\mathcal{O}(\alpha_{em}^4 \alpha_s^2)$ for the study of the quartic electroweak gauge boson vertex at CERN LHC", *Phys. Rev. D* **74** (2006) 073005, `doi:10.1103/PhysRevD.74.073005`, `arXiv:hep-ph/0606118`.

[7] CMS Collaboration, "Search for anomalous triple gauge couplings in WW and WZ production in lepton + jet events in proton-proton collisions at $\sqrt{s}$ 13 TeV", *JHEP* **12** (2019) 062, `doi:10.1007/JHEP12(2019)062`, `arXiv:1907.08354`.

[8] ATLAS Collaboration, "Evidence for electroweak production of two jets in association with a Z pair in pp collisions at $\sqrt{s}$ 13 TeV with the ATLAS detector", *Phys. Lett. B* **803** (2020) 135341, `doi:10.1016/j.physletb.2020.135341`, `arXiv:1910.09503`.

[9] CMS Collaboration, "Measurement of the cross section for electroweak production of a Z boson, a photon and two jets in proton-proton collisions at $\sqrt{s}$ 13 TeV and constraints on anomalous quartic couplings", *JHEP* **06** (2020) 076, `doi:10.1007/JHEP06(2020)076`, `arXiv:2002.09902`.

[10] CMS Collaboration, "The CMS experiment at the CERN LHC", *JINST* **3** (2008) S08004, `doi:10.1088/1748-0221/3/08/S08004`.

[11] CMS Collaboration, "The CMS trigger system", *JINST* **12** (2017) P01020, `doi:10.1088/1748-0221/12/01/P01020`, `arXiv:1609.02366`.

[12] J. Alwall et al., "The automated computation of tree-level and next-to-leading order differential cross sections, and their matching to parton shower simulations", *JHEP* **07** (2014) 079, `doi:10.1007/JHEP07(2014)079`, `arXiv:1405.0301`.

[13] T. Melia, P. Nason, R. Rontsch, and G. Zanderighi, "W W , WZ and ZZ production in the POWHEG BOX", *JHEP* **11** (2011) 078, `doi:10.1007/JHEP11(2011)078`, `arXiv:1107.5051`.

[14] P. Nason, "A new method for combining NLO QCD with shower Monte Carlo algorithms", *JHEP* **11** (2004) 040, `doi:10.1088/1126-6708/2004/11/040`, `arXiv:hep-ph/0409146`.

[15] S. Frixione, P. Nason, and C. Oleari, "Matching NLO QCD computations with parton shower simulations: the POWHEG method", *JHEP* **11** (2007) 070, `doi:10.1088/1126-6708/2007/11/070`, `arXiv:0709.2092`.

[16] S. Alioli, P. Nason, C. Oleari, and E. Re, "A general framework for implementing NLO calculations in shower Monte Carlo programs: the POWHEG BOX", *JHEP* **06** (2010) 043, `doi:10.1007/JHEP06(2010)043`, `arXiv:1002.2581`.

[17] T. Sjöstrand et al., "An introduction to PYTHIA 8.2", *Comput. Phys. Commun.* **191** (2015) 159, `doi:10.1016/j.cpc.2015.01.024`, `arXiv:1410.3012`.

[18] R. Frederix and S. Frixione, "Merging meets matching in MC@NLO", *JHEP* **12** (2012) 061, `doi:10.1007/JHEP12(2012)061`, `arXiv:1209.6215`.

[19] O. Mattelaer, "On the maximal use of Monte Carlo samples: re-weighting events at NLO accuracy", *Eur. Phys. J. C* **76** (2016) 674, `doi:10.1140/epjc/s10052-016-4533-7`, `arXiv:1607.00763`.

[20] NNPDF Collaboration, "Parton distributions for the LHC run II", *JHEP* **04** (2015) 040, `doi:10.1007/JHEP04(2015)040`, `arXiv:1410.8849`.

[21] NNPDF Collaboration, "Parton distributions from high-precision collider data", *Eur. Phys. J. C* **77** (2017) 663, `doi:10.1140/epjc/s10052-017-5199-5`, `arXiv:1706.00428`.

[22] P. Skands, S. Carrazza, and J. Rojo, "Tuning PYTHIA 8.1: the Monash 2013 tune", *Eur. Phys. J. C* **74** (2014) 3024, `doi:10.1140/epjc/s10052-014-3024-y`, `arXiv:1404.5630`.

[23] CMS Collaboration, "Event generator tunes obtained from underlying event and multiparton scattering measurements", *Eur. Phys. J. C* **76** (2016) 155, `doi:10.1140/epjc/s10052-016-3988-x`, `arXiv:1512.00815`.

[24] GEANT4 Collaboration, "GEANT4–a simulation toolkit", *Nucl. Instrum. Meth. A* **506** (2003) 250, `doi:10.1016/S0168-9002(03)01368-8`.

[25] GEANT4 Collaboration, "GEANT4 developments and applications", *IEEE Trans. Nucl. Sci.* **53** (2006) 270, `doi:10.1109/TNS.2006.869826`.

[26] CMS Collaboration, "Particle-flow reconstruction and global event description with the CMS detector", *JINST* **12** (2017) P10003, `doi:10.1088/1748-0221/12/10/P10003`, `arXiv:1706.04965`.

[27] M. Cacciari, G. P. Salam, and G. Soyez, "The anti-k_T jet clustering algorithm", *JHEP* **04** (2008) 063, `doi:10.1088/1126-6708/2008/04/063`, `arXiv:0802.1189`.

[28] M. Cacciari, G. P. Salam, and G. Soyez, "FastJet user manual", *Eur. Phys. J. C* **72** (2012) 1896, `doi:10.1140/epjc/s10052-012-1896-2`, `arXiv:1111.6097`.

[29] CMS Collaboration, "Electron and photon reconstruction and identification with the CMS experiment at the CERN LHC", *JINST* **16** (2021) P05014, `doi:10.1088/1748-0221/16/05/P05014`, `arXiv:2012.06888`.

[30] CMS Collaboration, "Performance of electron reconstruction and selection with the CMS detector in proton-proton collisions at $\sqrt{s}$ 8 TeV", *JINST* **10** (2015) P06005, `doi:10.1088/1748-0221/10/06/P06005`, `arXiv:1502.02701`.

[31] CMS Collaboration, "Performance of the CMS muon detector and muon reconstruction with proton-proton collisions at $\sqrt{s}$ 13 TeV", *JINST* **13** (2018) P06015, `doi:10.1088/1748-0221/13/06/P06015`, `arXiv:1804.04528`.

[32] M. Cacciari and G. P. Salam, "Pileup subtraction using jet areas", *Phys. Lett. B* **659** (2008) 119, `doi:10.1016/j.physletb.2007.09.077`, `arXiv:0707.1378`.

[33] CMS Collaboration, "Measurement of the inclusive W and Z production cross sections in pp collisions at $\sqrt{s}$ 7 TeV with the CMS experiment", *JHEP* **10** (2011) 132, `doi:10.1007/JHEP10(2011)132`, `arXiv:1107.4789`.

[34] CMS Collaboration, "Energy calibration and resolution of the CMS electromagnetic calorimeter in pp collision at $\sqrt{s}$ 7 TeV", *JINST* **8** (2013) P09009, `doi:10.1088/1748-0221/8/09/P09009`, `arXiv:1306.2016`.

[35] CMS Collaboration, "Performance of photon reconstruction and identification with the CMS detector in proton-proton collisions at $\sqrt{s}$ 8 TeV", *JINST* **10** (2015) P08010, `doi:10.1088/1748-0221/10/08/P08010`, `arXiv:1502.02702`.

[36] CMS Collaboration, "Jet energy scale and resolution in the CMS experiment in pp collisions at 8 TeV", *JINST* **12** (2017) P02014, `doi:10.1088/1748-0221/12/02/P02014`, `arXiv:1607.03663`.

[37] CMS Collaboration, "Pileup mitigation at CMS in 13 TeV data", *JINST* **15** (2020) P09018, `doi:10.1088/1748-0221/15/09/P09018`, `arXiv:2003.00503`.

[38] D. Rainwater, R. Szalapski, and D. Zeppenfeld, "Probing color singlet exchange in Z+2-jet events at the CERN LHC", *Phys. Rev. D* **54** (1996) 6680, `doi:10.1103/PhysRevD.54.6680`, `arXiv:hep-ph/9605444`.

[39] N. Kidonakis, "Two-loop soft anomalous dimensions for single top quark associated production with a W or H ", *Phys. Rev. D* **82** (2010) 054018, `doi:10.1103/PhysRevD.82.054018`, `arXiv:1005.4451`.

[40] J. Butterworth et al., "PDF4LHC recommendations for LHC Run II", *J. Phys. G* **43** (2016) 023001, `doi:10.1088/0954-3899/43/2/023001`, `arXiv:1510.03865`.

[41] CMS Collaboration, "Measurement of the inelastic proton-proton cross section at $\sqrt{s}$ 13 TeV", *JHEP* **07** (2018) 161, `doi:10.1007/JHEP07(2018)161`, `arXiv:1802.02613`.

[42] CMS Collaboration, "Precision luminosity measurement in proton-proton collisions at $\sqrt{s}$ 13 TeV in 2015 and 2016 at CMS", 2021. `arXiv:2104.01927`. Submitted to *Eur. Phys. J. C*.

[43] CMS Collaboration, "CMS luminosity measurement for the 2017 data-taking period at $\sqrt{s}$ 13 TeV", Physics Analysis Summary CMS-PAS-LUM-17-004, CERN, Geneva, 2018.

[44] CMS Collaboration, "CMS luminosity measurement for the 2018 data-taking period at $\sqrt{s}$ 13 TeV", Physics Analysis Summary CMS-PAS-LUM-18-002, CERN, Geneva, 2019.

[45] L. Demortier, "P values and nuisance parameters", in *Statistical issues for LHC physics. Proceedings, Workshop, PHYSTAT-LHC, Geneva, Switzerland, June 27-29, 2007*. 2008. `doi:10.5170/CERN-2008-001`.

[46] G. Cowan, K. Cranmer, E. Gross, and O. Vitells, "Asymptotic formulae for likelihood-based tests of new physics", *Eur. Phys. J. C* **71** (2011) 1554, `doi:10.1140/epjc/s10052-011-1554-0`, `arXiv:1007.1727`. [Erratum: `doi:10.1140/epjc/s10052-013-2501-z`].

[47] P. C. Hansen, "Computational aspects: Regularization methods", in *Discrete inverse problems: insight and algorithms*. SIAM, 2010. `doi:10.1137/1.9780898718836.ch4`.

[48] S. S. Wilks, "The large-sample distribution of the likelihood ratio for testing composite hypotheses", *Ann. Math. Statist* **9** (1938) 60, `doi:10.1214/aoms/1177732360`.

[49] CMS Collaboration, "Precise determination of the mass of the Higgs boson and tests of compatibility of its couplings with the standard model predictions using proton collisions at 7 and 8 TeV", *Eur. Phys. J. C* **75** (2015) 212, `doi:10.1140/epjc/s10052-015-3351-7`, `arXiv:1412.8662`.

[50] E. d. S. Almeida, O. J. P. Éboli, and M. C. Gonzalez–Garcia, "Unitarity constraints on anomalous quartic couplings", *Phys. Rev. D* **101** (2020) 113003, `doi:10.1103/PhysRevD.101.113003`, `arXiv:2004.05174`.

A The CMS Collaboration

Yerevan Physics Institute, Yerevan, Armenia
A. Tumasyan

Institut für Hochenergiephysik, Wien, Austria
W. Adam, J.W. Andrejkovic, T. Bergauer, S. Chatterjee, M. Dragicevic, A. Escalante Del Valle, R. Frühwirth[1], M. Jeitler[1], N. Krammer, L. Lechner, D. Liko, I. Mikulec, P. Paulitsch, F.M. Pitters, J. Schieck[1], R. Schöfbeck, M. Spanring, S. Templ, W. Waltenberger, C.-E. Wulz[1]

Institute for Nuclear Problems, Minsk, Belarus
V. Chekhovsky, A. Litomin, V. Makarenko

Universiteit Antwerpen, Antwerpen, Belgium
M.R. Darwish[2], E.A. De Wolf, T. Janssen, T. Kello[3], A. Lelek, H. Rejeb Sfar, P. Van Mechelen, S. Van Putte, N. Van Remortel

Vrije Universiteit Brussel, Brussel, Belgium
F. Blekman, E.S. Bols, J. D'Hondt, M. Delcourt, H. El Faham, S. Lowette, S. Moortgat, A. Morton, D. Müller, A.R. Sahasransu, S. Tavernier, W. Van Doninck, P. Van Mulders

Université Libre de Bruxelles, Bruxelles, Belgium
D. Beghin, B. Bilin, B. Clerbaux, G. De Lentdecker, L. Favart, A. Grebenyuk, A.K. Kalsi, K. Lee, M. Mahdavikhorrami, I. Makarenko, L. Moureaux, L. Pétré, A. Popov, N. Postiau, E. Starling, L. Thomas, M. Vanden Bemden, C. Vander Velde, P. Vanlaer, D. Vannerom, L. Wezenbeek

Ghent University, Ghent, Belgium
T. Cornelis, D. Dobur, J. Knolle, L. Lambrecht, G. Mestdach, M. Niedziela, C. Roskas, A. Samalan, K. Skovpen, M. Tytgat, W. Verbeke, B. Vermassen, M. Vit

Université Catholique de Louvain, Louvain-la-Neuve, Belgium
A. Bethani, G. Bruno, F. Bury, C. Caputo, P. David, C. Delaere, I.S. Donertas, A. Giammanco, K. Jaffel, Sa. Jain, V. Lemaitre, K. Mondal, J. Prisciandaro, A. Taliercio, M. Teklishyn, T.T. Tran, P. Vischia, S. Wertz

Centro Brasileiro de Pesquisas Fisicas, Rio de Janeiro, Brazil
G.A. Alves, C. Hensel, A. Moraes

Universidade do Estado do Rio de Janeiro, Rio de Janeiro, Brazil
W.L. Aldá Júnior, M. Alves Gallo Pereira, M. Barroso Ferreira Filho, H. BRANDAO MAL-BOUISSON, W. Carvalho, J. Chinellato[4], E.M. Da Costa, G.G. Da Silveira[5], D. De Jesus Damiao, S. Fonseca De Souza, D. Matos Figueiredo, C. Mora Herrera, K. Mota Amarilo, L. Mundim, H. Nogima, P. Rebello Teles, A. Santoro, S.M. Silva Do Amaral, A. Sznajder, M. Thiel, F. Torres Da Silva De Araujo, A. Vilela Pereira

Universidade Estadual Paulista [a], Universidade Federal do ABC [b], São Paulo, Brazil
C.A. Bernardes[a,a,5], L. Calligaris[a], T.R. Fernandez Perez Tomei[a], E.M. Gregores[a,b], D.S. Lemos[a], P.G. Mercadante[a,b], S.F. Novaes[a], Sandra S. Padula[a]

Institute for Nuclear Research and Nuclear Energy, Bulgarian Academy of Sciences, Sofia, Bulgaria
A. Aleksandrov, G. Antchev, R. Hadjiiska, P. Iaydjiev, M. Misheva, M. Rodozov, M. Shopova, G. Sultanov

University of Sofia, Sofia, Bulgaria
A. Dimitrov, T. Ivanov, L. Litov, B. Pavlov, P. Petkov, A. Petrov

Beihang University, Beijing, China
T. Cheng, Q. Guo, T. Javaid[6], M. Mittal, H. Wang, L. Yuan

Department of Physics, Tsinghua University, Beijing, China
M. Ahmad, G. Bauer, C. Dozen[7], Z. Hu, J. Martins[8], Y. Wang, K. Yi[9,10]

Institute of High Energy Physics, Beijing, China
E. Chapon, G.M. Chen[6], H.S. Chen[6], M. Chen, F. Iemmi, A. Kapoor, D. Leggat, H. Liao, Z.-A. LIU[6], V. Milosevic, F. Monti, R. Sharma, J. Tao, J. Thomas-wilsker, J. Wang, H. Zhang, S. Zhang[6], J. Zhao

State Key Laboratory of Nuclear Physics and Technology, Peking University, Beijing, China
A. Agapitos, Y. An, Y. Ban, C. Chen, A. Levin, Q. Li, X. Lyu, Y. Mao, S.J. Qian, D. Wang, Q. Wang, J. Xiao

Sun Yat-Sen University, Guangzhou, China
M. Lu, Z. You

Institute of Modern Physics and Key Laboratory of Nuclear Physics and Ion-beam Application (MOE) - Fudan University, Shanghai, China
X. Gao[3], H. Okawa

Zhejiang University, Hangzhou, China
Z. Lin, M. Xiao

Universidad de Los Andes, Bogota, Colombia
C. Avila, A. Cabrera, C. Florez, J. Fraga

Universidad de Antioquia, Medellin, Colombia
J. Mejia Guisao, F. Ramirez, J.D. Ruiz Alvarez, C.A. Salazar González

University of Split, Faculty of Electrical Engineering, Mechanical Engineering and Naval Architecture, Split, Croatia
D. Giljanovic, N. Godinovic, D. Lelas, I. Puljak

University of Split, Faculty of Science, Split, Croatia
Z. Antunovic, M. Kovac, T. Sculac

Institute Rudjer Boskovic, Zagreb, Croatia
V. Brigljevic, D. Ferencek, D. Majumder, M. Roguljic, A. Starodumov[11], T. Susa

University of Cyprus, Nicosia, Cyprus
A. Attikis, K. Christoforou, E. Erodotou, A. Ioannou, G. Kole, M. Kolosova, S. Konstantinou, J. Mousa, C. Nicolaou, F. Ptochos, P.A. Razis, H. Rykaczewski, H. Saka

Charles University, Prague, Czech Republic
M. Finger[12], M. Finger Jr.[12], A. Kveton

Escuela Politecnica Nacional, Quito, Ecuador
E. Ayala

Universidad San Francisco de Quito, Quito, Ecuador
E. Carrera Jarrin

Academy of Scientific Research and Technology of the Arab Republic of Egypt, Egyptian Network of High Energy Physics, Cairo, Egypt
A.A. Abdelalim[13,14], A. Ellithi Kamel[15,15] A. Ellithi Kamel[15,15]

Center for High Energy Physics (CHEP-FU), Fayoum University, El-Fayoum, Egypt
A. Lotfy, M.A. Mahmoud

National Institute of Chemical Physics and Biophysics, Tallinn, Estonia
S. Bhowmik, R.K. Dewanjee, K. Ehataht, M. Kadastik, S. Nandan, C. Nielsen, J. Pata, M. Raidal, L. Tani, C. Veelken

Department of Physics, University of Helsinki, Helsinki, Finland
P. Eerola, L. Forthomme, H. Kirschenmann, K. Osterberg, M. Voutilainen

Helsinki Institute of Physics, Helsinki, Finland
S. Bharthuar, E. Brücken, F. Garcia, J. Havukainen, M.S. Kim, R. Kinnunen, T. Lampén, K. Lassila-Perini, S. Lehti, T. Lindén, M. Lotti, L. Martikainen, M. Myllymäki, J. Ott, H. Siikonen, E. Tuominen, J. Tuominiemi

Lappeenranta University of Technology, Lappeenranta, Finland
P. Luukka, H. Petrow, T. Tuuva

IRFU, CEA, Université Paris-Saclay, Gif-sur-Yvette, France
C. Amendola, M. Besancon, F. Couderc, M. Dejardin, D. Denegri, J.L. Faure, F. Ferri, S. Ganjour, A. Givernaud, P. Gras, G. Hamel de Monchenault, P. Jarry, B. Lenzi, E. Locci, J. Malcles, J. Rander, A. Rosowsky, M.Ö. Sahin, A. Savoy-Navarro[16], M. Titov, G.B. Yu

Laboratoire Leprince-Ringuet, CNRS/IN2P3, Ecole Polytechnique, Institut Polytechnique de Paris, Palaiseau, France
S. Ahuja, F. Beaudette, M. Bonanomi, A. Buchot Perraguin, P. Busson, A. Cappati, C. Charlot, O. Davignon, B. Diab, G. Falmagne, S. Ghosh, R. Granier de Cassagnac, A. Hakimi, I. Kucher, J. Motta, M. Nguyen, C. Ochando, P. Paganini, J. Rembser, R. Salerno, J.B. Sauvan, Y. Sirois, A. Tarabini, A. Zabi, A. Zghiche

Université de Strasbourg, CNRS, IPHC UMR 7178, Strasbourg, France
J.-L. Agram[17], J. Andrea, D. Apparu, D. Bloch, G. Bourgatte, J.-M. Brom, E.C. Chabert, C. Collard, D. Darej, J.-C. Fontaine[17], U. Goerlach, C. Grimault, A.-C. Le Bihan, E. Nibigira, P. Van Hove

Institut de Physique des 2 Infinis de Lyon (IP2I), Villeurbanne, France
E. Asilar, S. Beauceron, C. Bernet, G. Boudoul, C. Camen, A. Carle, N. Chanon, D. Contardo, P. Depasse, H. El Mamouni, J. Fay, S. Gascon, M. Gouzevitch, B. Ille, I.B. Laktineh, H. Lattaud, A. Lesauvage, M. Lethuillier, L. Mirabito, S. Perries, K. Shchablo, V. Sordini, L. Torterotot, G. Touquet, M. Vander Donckt, S. Viret

Georgian Technical University, Tbilisi, Georgia
I. Lomidze, T. Toriashvili[18], Z. Tsamalaidze[12]

RWTH Aachen University, I. Physikalisches Institut, Aachen, Germany
L. Feld, K. Klein, M. Lipinski, D. Meuser, A. Pauls, M.P. Rauch, N. Röwert, J. Schulz, M. Teroerde

RWTH Aachen University, III. Physikalisches Institut A, Aachen, Germany
A. Dodonova, D. Eliseev, M. Erdmann, P. Fackeldey, B. Fischer, S. Ghosh, T. Hebbeker, K. Hoepfner, F. Ivone, H. Keller, L. Mastrolorenzo, M. Merschmeyer, A. Meyer, G. Mocellin, S. Mondal, S. Mukherjee, D. Noll, A. Novak, T. Pook, A. Pozdnyakov, Y. Rath, H. Reithler, J. Roemer, A. Schmidt, S.C. Schuler, A. Sharma, L. Vigilante, S. Wiedenbeck, S. Zaleski

RWTH Aachen University, III. Physikalisches Institut B, Aachen, Germany
C. Dziwok, G. Flügge, W. Haj Ahmad[19], O. Hlushchenko, T. Kress, A. Nowack, C. Pistone, O. Pooth, D. Roy, H. Sert, A. Stahl[20], T. Ziemons

Deutsches Elektronen-Synchrotron, Hamburg, Germany
H. Aarup Petersen, M. Aldaya Martin, P. Asmuss, I. Babounikau, S. Baxter, O. Behnke, A. Bermúdez Martínez, S. Bhattacharya, A.A. Bin Anuar, K. Borras[21], V. Botta, D. Brunner, A. Campbell, A. Cardini, C. Cheng, F. Colombina, S. Consuegra Rodríguez, G. Correia Silva, V. Danilov, L. Didukh, G. Eckerlin, D. Eckstein, L.I. Estevez Banos, O. Filatov, E. Gallo[22], A. Geiser, A. Giraldi, A. Grohsjean, M. Guthoff, A. Jafari[23], N.Z. Jomhari, H. Jung, A. Kasem[21], M. Kasemann, H. Kaveh, C. Kleinwort, D. Krücker, W. Lange, J. Lidrych, K. Lipka, W. Lohmann[24], R. Mankel, I.-A. Melzer-Pellmann, M. Mendizabal Morentin, J. Metwally, A.B. Meyer, M. Meyer, J. Mnich, A. Mussgiller, Y. Otarid, D. Pérez Adán, D. Pitzl, A. Raspereza, B. Ribeiro Lopes, J. Rübenach, A. Saggio, A. Saibel, M. Savitskyi, M. Scham, V. Scheurer, P. Schütze, C. Schwanenberger[22], A. Singh, R.E. Sosa Ricardo, D. Stafford, N. Tonon, O. Turkot, M. Van De Klundert, R. Walsh, D. Walter, Y. Wen, K. Wichmann, L. Wiens, C. Wissing, S. Wuchterl

University of Hamburg, Hamburg, Germany
R. Aggleton, S. Albrecht, S. Bein, L. Benato, A. Benecke, P. Connor, K. De Leo, M. Eich, F. Feindt, A. Fröhlich, C. Garbers, E. Garutti, P. Gunnellini, J. Haller, A. Hinzmann, G. Kasieczka, R. Klanner, R. Kogler, T. Kramer, V. Kutzner, J. Lange, T. Lange, A. Lobanov, A. Malara, A. Nigamova, K.J. Pena Rodriguez, O. Rieger, P. Schleper, M. Schröder, J. Schwandt, D. Schwarz, J. Sonneveld, H. Stadie, G. Steinbrück, A. Tews, B. Vormwald, I. Zoi

Karlsruher Institut fuer Technologie, Karlsruhe, Germany
J. Bechtel, T. Berger, E. Butz, R. Caspart, T. Chwalek, W. De Boer[†], A. Dierlamm, A. Droll, K. El Morabit, N. Faltermann, M. Giffels, J.o. Gosewisch, A. Gottmann, F. Hartmann[20], C. Heidecker, U. Husemann, P. Keicher, R. Koppenhöfer, S. Maier, M. Metzler, S. Mitra, Th. Müller, M. Neukum, A. Nürnberg, G. Quast, K. Rabbertz, J. Rauser, D. Savoiu, M. Schnepf, D. Seith, I. Shvetsov, H.J. Simonis, R. Ulrich, J. Van Der Linden, R.F. Von Cube, M. Wassmer, M. Weber, S. Wieland, R. Wolf, S. Wozniewski, S. Wunsch

Institute of Nuclear and Particle Physics (INPP), NCSR Demokritos, Aghia Paraskevi, Greece
G. Anagnostou, G. Daskalakis, T. Geralis, A. Kyriakis, D. Loukas, A. Stakia

National and Kapodistrian University of Athens, Athens, Greece
M. Diamantopoulou, D. Karasavvas, G. Karathanasis, P. Kontaxakis, C.K. Koraka, A. Manousakis-katsikakis, A. Panagiotou, I. Papavergou, N. Saoulidou, K. Theofilatos, E. Tziaferi, K. Vellidis, E. Vourliotis

National Technical University of Athens, Athens, Greece
G. Bakas, K. Kousouris, I. Papakrivopoulos, G. Tsipolitis, A. Zacharopoulou

University of Ioánnina, Ioánnina, Greece
I. Evangelou, C. Foudas, P. Gianneios, P. Katsoulis, P. Kokkas, N. Manthos, I. Papadopoulos, J. Strologas

MTA-ELTE Lendület CMS Particle and Nuclear Physics Group, Eötvös Loránd University, Budapest, Hungary
M. Csanad, K. Farkas, M.M.A. Gadallah[25], S. Lökös[26], P. Major, K. Mandal, A. Mehta, G. Pasztor, A.J. Rádl, O. Surányi, G.I. Veres

Wigner Research Centre for Physics, Budapest, Hungary
M. Bartók[27], G. Bencze, C. Hajdu, D. Horvath[28], F. Sikler, V. Veszpremi, G. Vesztergombi[†]

Institute of Nuclear Research ATOMKI, Debrecen, Hungary
S. Czellar, J. Karancsi[27], J. Molnar, Z. Szillasi, D. Teyssier

Institute of Physics, University of Debrecen, Debrecen, Hungary
P. Raics, Z.L. Trocsanyi[29], B. Ujvari

Karoly Robert Campus, MATE Institute of Technology
T. Csorgo[30], F. Nemes[30], T. Novak

Indian Institute of Science (IISc), Bangalore, India
J.R. Komaragiri, D. Kumar, L. Panwar, P.C. Tiwari

National Institute of Science Education and Research, HBNI, Bhubaneswar, India
S. Bahinipati[31], C. Kar, P. Mal, T. Mishra, V.K. Muraleedharan Nair Bindhu[32], A. Nayak[32], P. Saha, N. Sur, S.K. Swain, D. Vats[32]

Panjab University, Chandigarh, India
S. Bansal, S.B. Beri, V. Bhatnagar, G. Chaudhary, S. Chauhan, N. Dhingra[33], R. Gupta, A. Kaur, M. Kaur, S. Kaur, P. Kumari, M. Meena, K. Sandeep, J.B. Singh, A.K. Virdi

University of Delhi, Delhi, India
A. Ahmed, A. Bhardwaj, B.C. Choudhary, M. Gola, S. Keshri, A. Kumar, M. Naimuddin, P. Priyanka, K. Ranjan, A. Shah

Saha Institute of Nuclear Physics, HBNI, Kolkata, India
M. Bharti[34], R. Bhattacharya, S. Bhattacharya, D. Bhowmik, S. Dutta, S. Dutta, B. Gomber[35], M. Maity[36], P. Palit, P.K. Rout, G. Saha, B. Sahu, S. Sarkar, M. Sharan, B. Singh[34], S. Thakur[34]

Indian Institute of Technology Madras, Madras, India
P.K. Behera, S.C. Behera, P. Kalbhor, A. Muhammad, R. Pradhan, P.R. Pujahari, A. Sharma, A.K. Sikdar

Bhabha Atomic Research Centre, Mumbai, India
D. Dutta, V. Jha, V. Kumar, D.K. Mishra, K. Naskar[37], P.K. Netrakanti, L.M. Pant, P. Shukla

Tata Institute of Fundamental Research-A, Mumbai, India
T. Aziz, S. Dugad, M. Kumar, U. Sarkar

Tata Institute of Fundamental Research-B, Mumbai, India
S. Banerjee, R. Chudasama, M. Guchait, S. Karmakar, S. Kumar, G. Majumder, K. Mazumdar, S. Mukherjee

Indian Institute of Science Education and Research (IISER), Pune, India
K. Alpana, S. Dube, B. Kansal, A. Laha, S. Pandey, A. Rane, A. Rastogi, S. Sharma

Department of Physics, Isfahan University of Technology, Isfahan, Iran
H. Bakhshiansohi[38], M. Zeinali[39]

Institute for Research in Fundamental Sciences (IPM), Tehran, Iran
S. Chenarani[40], S.M. Etesami, M. Khakzad, M. Mohammadi Najafabadi

University College Dublin, Dublin, Ireland
M. Grunewald

INFN Sezione di Bari [a], Università di Bari [b], Politecnico di Bari [c], Bari, Italy

M. Abbrescia[a,b], R. Aly[a,b,41], C. Aruta[a,b], A. Colaleo[a], D. Creanza[a,c], N. De Filippis[a,c], M. De Palma[a,b], A. Di Florio[a,b], A. Di Pilato[a,b], W. Elmetenawee[a,b], L. Fiore[a], A. Gelmi[a,b], M. Gul[a], G. Iaselli[a,c], M. Ince[a,b], S. Lezki[a,b], G. Maggi[a,c], M. Maggi[a], I. Margjeka[a,b], V. Mastrapasqua[a,b], J.A. Merlin[a], S. My[a,b], S. Nuzzo[a,b], A. Pellecchia[a,b], A. Pompili[a,b], G. Pugliese[a,c], A. Ranieri[a], G. Selvaggi[a,b], L. Silvestris[a], F.M. Simone[a,b], R. Venditti[a], P. Verwilligen[a]

INFN Sezione di Bologna [a], Università di Bologna [b], Bologna, Italy

G. Abbiendi[a], C. Battilana[a,b], D. Bonacorsi[a,b], L. Borgonovi[a], L. Brigliadori[a], R. Campanini[a,b], P. Capiluppi[a,b], A. Castro[a,b], F.R. Cavallo[a], M. Cuffiani[a,b], G.M. Dallavalle[a], T. Diotalevi[a,b], F. Fabbri[a], A. Fanfani[a,b], P. Giacomelli[a], L. Giommi[a,b], C. Grandi[a], L. Guiducci[a,b], S. Lo Meo[a,42], L. Lunerti[a,b], S. Marcellini[a], G. Masetti[a], F.L. Navarria[a,b], A. Perrotta[a], F. Primavera[a,b], A.M. Rossi[a,b], T. Rovelli[a,b], G.P. Siroli[a,b]

INFN Sezione di Catania [a], Università di Catania [b], Catania, Italy

S. Albergo[a,b,43], S. Costa[a,b,43], A. Di Mattia[a], R. Potenza[a,b], A. Tricomi[a,b,43], C. Tuve[a,b]

INFN Sezione di Firenze [a], Università di Firenze [b], Firenze, Italy

G. Barbagli[a], A. Cassese[a], R. Ceccarelli[a,b], V. Ciulli[a,b], C. Civinini[a], R. D'Alessandro[a,b], E. Focardi[a,b], G. Latino[a,b], P. Lenzi[a,b], M. Lizzo[a,b], M. Meschini[a], S. Paoletti[a], R. Seidita[a,b], G. Sguazzoni[a], L. Viliani[a]

INFN Laboratori Nazionali di Frascati, Frascati, Italy

L. Benussi, S. Bianco, D. Piccolo

INFN Sezione di Genova [a], Università di Genova [b], Genova, Italy

M. Bozzo[a,b], F. Ferro[a], R. Mulargia[a,b], E. Robutti[a], S. Tosi[a,b]

INFN Sezione di Milano-Bicocca [a], Università di Milano-Bicocca [b], Milano, Italy

A. Benaglia[a], F. Brivio[a,b], F. Cetorelli[a,b], V. Ciriolo[a,b,20], F. De Guio[a,b], M.E. Dinardo[a,b], P. Dini[a], S. Gennai[a], A. Ghezzi[a,b], P. Govoni[a,b], L. Guzzi[a,b], M. Malberti[a], S. Malvezzi[a], A. Massironi[a], D. Menasce[a], L. Moroni[a], M. Paganoni[a,b], D. Pedrini[a], S. Ragazzi[a,b], N. Redaelli[a], T. Tabarelli de Fatis[a,b], D. Valsecchi[a,b,20], D. Zuolo[a,b]

INFN Sezione di Napoli [a], Università di Napoli 'Federico II' [b], Napoli, Italy, Università della Basilicata [c], Potenza, Italy, Università G. Marconi [d], Roma, Italy

S. Buontempo[a], F. Carnevali[a,b], N. Cavallo[a,c], A. De Iorio[a,b], F. Fabozzi[a,c], A.O.M. Iorio[a,b], L. Lista[a,b], S. Meola[a,d,20], P. Paolucci[a,20], B. Rossi[a], C. Sciacca[a,b]

INFN Sezione di Padova [a], Università di Padova [b], Padova, Italy, Università di Trento [c], Trento, Italy

P. Azzi[a], N. Bacchetta[a], D. Bisello[a,b], P. Bortignon[a], A. Bragagnolo[a,b], R. Carlin[a,b], P. Checchia[a], T. Dorigo[a], U. Dosselli[a], F. Gasparini[a,b], U. Gasparini[a,b], S.Y. Hoh[a,b], L. Layer[a,44], M. Margoni[a,b], A.T. Meneguzzo[a,b], J. Pazzini[a,b], M. Presilla[a,b], P. Ronchese[a,b], R. Rossin[a,b], F. Simonetto[a,b], G. Strong[a], M. Tosi[a,b], H. YARAR[a,b], M. Zanetti[a,b], P. Zotto[a,b], A. Zucchetta[a,b], G. Zumerle[a,b]

INFN Sezione di Pavia [a], Università di Pavia [b], Pavia, Italy

C. Aime'[a,b], A. Braghieri[a], S. Calzaferri[a,b], D. Fiorina[a,b], P. Montagna[a,b], S.P. Ratti[a,b], V. Re[a], C. Riccardi[a,b], P. Salvini[a], I. Vai[a], P. Vitulo[a,b]

INFN Sezione di Perugia [a], Università di Perugia [b], Perugia, Italy

P. Asenov[a,45], G.M. Bilei[a], D. Ciangottini[a,b], L. Fanò[a,b], P. Lariccia[a,b], M. Magherini[b],

G. Mantovani[a,b], V. Mariani[a,b], M. Menichelli[a], F. Moscatelli[a,45], A. Piccinelli[a,b], A. Rossi[a,b], A. Santocchia[a,b], D. Spiga[a], T. Tedeschi[a,b]

INFN Sezione di Pisa [a], Università di Pisa [b], Scuola Normale Superiore di Pisa [c], Pisa Italy, Università di Siena [d], Siena, Italy
P. Azzurri[a], G. Bagliesi[a], V. Bertacchi[a,c], L. Bianchini[a], T. Boccali[a], E. Bossini[a,b], R. Castaldi[a], M.A. Ciocci[a,b], V. D'Amante[a,d], R. Dell'Orso[a], M.R. Di Domenico[a,d], S. Donato[a], A. Giassi[a], F. Ligabue[a,c], E. Manca[a,c], G. Mandorli[a,c], A. Messineo[a,b], F. Palla[a], S. Parolia[a,b], G. Ramirez-Sanchez[a,c], A. Rizzi[a,b], G. Rolandi[a,c], S. Roy Chowdhury[a,c], A. Scribano[a], N. Shafiei[a,b], P. Spagnolo[a], R. Tenchini[a], G. Tonelli[a,b], N. Turini[a,d], A. Venturi[a], P.G. Verdini[a]

INFN Sezione di Roma [a], Sapienza Università di Roma [b], Rome, Italy
M. Campana[a,b], F. Cavallari[a], D. Del Re[a,b], E. Di Marco[a], M. Diemoz[a], E. Longo[a,b], P. Meridiani[a], G. Organtini[a,b], F. Pandolfi[a], R. Paramatti[a,b], C. Quaranta[a,b], S. Rahatlou[a,b], C. Rovelli[a], F. Santanastasio[a,b], L. Soffi[a], R. Tramontano[a,b]

INFN Sezione di Torino [a], Università di Torino [b], Torino, Italy, Università del Piemonte Orientale [c], Novara, Italy
N. Amapane[a,b], R. Arcidiacono[a,c], S. Argiro[a,b], M. Arneodo[a,c], N. Bartosik[a], R. Bellan[a,b], A. Bellora[a,b], J. Berenguer Antequera[a,b], C. Biino[a], N. Cartiglia[a], S. Cometti[a], M. Costa[a,b], R. Covarelli[a,b], N. Demaria[a], B. Kiani[a,b], F. Legger[a], C. Mariotti[a], S. Maselli[a], E. Migliore[a,b], E. Monteil[a,b], M. Monteno[a], M.M. Obertino[a,b], G. Ortona[a], L. Pacher[a,b], N. Pastrone[a], M. Pelliccioni[a], G.L. Pinna Angioni[a,b], M. Ruspa[a,c], K. Shchelina[a,b], F. Siviero[a,b], V. Sola[a], A. Solano[a,b], D. Soldi[a,b], A. Staiano[a], M. Tornago[a,b], D. Trocino[a,b], A. Vagnerini

INFN Sezione di Trieste [a], Università di Trieste [b], Trieste, Italy
S. Belforte[a], V. Candelise[a,b], M. Casarsa[a], F. Cossutti[a], A. Da Rold[a,b], G. Della Ricca[a,b], G. Sorrentino[a,b], F. Vazzoler[a,b]

Kyungpook National University, Daegu, Korea
S. Dogra, C. Huh, B. Kim, D.H. Kim, G.N. Kim, J. Kim, J. Lee, S.W. Lee, C.S. Moon, Y.D. Oh, S.I. Pak, B.C. Radburn-Smith, S. Sekmen, Y.C. Yang

Chonnam National University, Institute for Universe and Elementary Particles, Kwangju, Korea
H. Kim, D.H. Moon

Hanyang University, Seoul, Korea
B. Francois, T.J. Kim, J. Park

Korea University, Seoul, Korea
S. Cho, S. Choi, Y. Go, B. Hong, K. Lee, K.S. Lee, J. Lim, J. Park, S.K. Park, J. Yoo

Kyung Hee University, Department of Physics, Seoul, Republic of Korea
J. Goh, A. Gurtu

Sejong University, Seoul, Korea
H.S. Kim, Y. Kim

Seoul National University, Seoul, Korea
J. Almond, J.H. Bhyun, J. Choi, S. Jeon, J. Kim, J.S. Kim, S. Ko, H. Kwon, H. Lee, S. Lee, B.H. Oh, M. Oh, S.B. Oh, H. Seo, U.K. Yang, I. Yoon

University of Seoul, Seoul, Korea
W. Jang, D.Y. Kang, Y. Kang, S. Kim, B. Ko, J.S.H. Lee, Y. Lee, I.C. Park, Y. Roh, M.S. Ryu, D. Song, I.J. Watson, S. Yang

Yonsei University, Department of Physics, Seoul, Korea
S. Ha, H.D. Yoo

Sungkyunkwan University, Suwon, Korea
M. Choi, Y. Jeong, H. Lee, Y. Lee, I. Yu

College of Engineering and Technology, American University of the Middle East (AUM), Egaila, Kuwait
T. Beyrouthy, Y. Maghrbi

Riga Technical University, Riga, Latvia
T. Torims, V. Veckalns[46]

Vilnius University, Vilnius, Lithuania
M. Ambrozas, A. Carvalho Antunes De Oliveira, A. Juodagalvis, A. Rinkevicius, G. Tamulaitis

National Centre for Particle Physics, Universiti Malaya, Kuala Lumpur, Malaysia
N. Bin Norjoharuddeen, W.A.T. Wan Abdullah, M.N. Yusli, Z. Zolkapli

Universidad de Sonora (UNISON), Hermosillo, Mexico
J.F. Benitez, A. Castaneda Hernandez, M. León Coello, J.A. Murillo Quijada, A. Sehrawat, L. Valencia Palomo

Centro de Investigacion y de Estudios Avanzados del IPN, Mexico City, Mexico
G. Ayala, H. Castilla-Valdez, E. De La Cruz-Burelo, I. Heredia-De La Cruz[47], R. Lopez-Fernandez, C.A. Mondragon Herrera, D.A. Perez Navarro, A. Sanchez-Hernandez

Universidad Iberoamericana, Mexico City, Mexico
S. Carrillo Moreno, C. Oropeza Barrera, F. Vazquez Valencia

Benemerita Universidad Autonoma de Puebla, Puebla, Mexico
I. Pedraza, H.A. Salazar Ibarguen, C. Uribe Estrada

University of Montenegro, Podgorica, Montenegro
J. Mijuskovic[48], N. Raicevic

University of Auckland, Auckland, New Zealand
D. Krofcheck

University of Canterbury, Christchurch, New Zealand
S. Bheesette, P.H. Butler

National Centre for Physics, Quaid-I-Azam University, Islamabad, Pakistan
A. Ahmad, M.I. Asghar, A. Awais, M.I.M. Awan, H.R. Hoorani, W.A. Khan, M.A. Shah, M. Shoaib, M. Waqas

AGH University of Science and Technology Faculty of Computer Science, Electronics and Telecommunications, Krakow, Poland
V. Avati, L. Grzanka, M. Malawski

National Centre for Nuclear Research, Swierk, Poland
H. Bialkowska, M. Bluj, B. Boimska, M. Górski, M. Kazana, M. Szleper, P. Zalewski

Institute of Experimental Physics, Faculty of Physics, University of Warsaw, Warsaw, Poland
K. Bunkowski, K. Doroba, A. Kalinowski, M. Konecki, J. Krolikowski, M. Walczak

Laboratório de Instrumentação e Física Experimental de Partículas, Lisboa, Portugal
M. Araujo, P. Bargassa, D. Bastos, A. Boletti, P. Faccioli, M. Gallinaro, J. Hollar, N. Leonardo, T. Niknejad, M. Pisano, J. Seixas, O. Toldaiev, J. Varela

Joint Institute for Nuclear Research, Dubna, Russia
S. Afanasiev, D. Budkouski, I. Golutvin, I. Gorbunov, V. Karjavine, V. Korenkov, A. Lanev, A. Malakhov, V. Matveev[49,50], V. Palichik, V. Perelygin, M. Savina, D. Seitova, V. Shalaev, S. Shmatov, S. Shulha, V. Smirnov, O. Teryaev, N. Voytishin, B.S. Yuldashev[51], A. Zarubin, I. Zhizhin

Petersburg Nuclear Physics Institute, Gatchina (St. Petersburg), Russia
G. Gavrilov, V. Golovtcov, Y. Ivanov, V. Kim[52], E. Kuznetsova[53], V. Murzin, V. Oreshkin, I. Smirnov, D. Sosnov, V. Sulimov, L. Uvarov, S. Volkov, A. Vorobyev

Institute for Nuclear Research, Moscow, Russia
Yu. Andreev, A. Dermenev, S. Gninenko, N. Golubev, A. Karneyeu, D. Kirpichnikov, M. Kirsanov, N. Krasnikov, A. Pashenkov, G. Pivovarov, D. Tlisov[†], A. Toropin

Institute for Theoretical and Experimental Physics named by A.I. Alikhanov of NRC 'Kurchatov Institute', Moscow, Russia
V. Epshteyn, V. Gavrilov, N. Lychkovskaya, A. Nikitenko[54], V. Popov, A. Spiridonov, A. Stepennov, M. Toms, E. Vlasov, A. Zhokin

Moscow Institute of Physics and Technology, Moscow, Russia
T. Aushev

National Research Nuclear University 'Moscow Engineering Physics Institute' (MEPhI), Moscow, Russia
O. Bychkova, M. Chadeeva[55], P. Parygin, E. Popova, V. Rusinov

P.N. Lebedev Physical Institute, Moscow, Russia
V. Andreev, M. Azarkin, I. Dremin, M. Kirakosyan, A. Terkulov

Skobeltsyn Institute of Nuclear Physics, Lomonosov Moscow State University, Moscow, Russia
A. Belyaev, E. Boos, M. Dubinin[56], L. Dudko, A. Gribushin, V. Klyukhin, O. Kodolova, I. Lokhtin, O. Lukina, S. Obraztsov, M. Perfilov, V. Savrin, A. Snigirev

Novosibirsk State University (NSU), Novosibirsk, Russia
V. Blinov[57], T. Dimova[57], L. Kardapoltsev[57], A. Kozyrev[57], I. Ovtin[57], Y. Skovpen[57]

Institute for High Energy Physics of National Research Centre 'Kurchatov Institute', Protvino, Russia
I. Azhgirey, I. Bayshev, D. Elumakhov, V. Kachanov, D. Konstantinov, P. Mandrik, V. Petrov, R. Ryutin, S. Slabospitskii, A. Sobol, S. Troshin, N. Tyurin, A. Uzunian, A. Volkov

National Research Tomsk Polytechnic University, Tomsk, Russia
A. Babaev, V. Okhotnikov

Tomsk State University, Tomsk, Russia
V. Borshch, V. Ivanchenko, E. Tcherniaev

University of Belgrade: Faculty of Physics and VINCA Institute of Nuclear Sciences, Belgrade, Serbia

P. Adzic[58], M. Dordevic, P. Milenovic, J. Milosevic

Centro de Investigaciones Energéticas Medioambientales y Tecnológicas (CIEMAT), Madrid, Spain

M. Aguilar-Benitez, J. Alcaraz Maestre, A. Álvarez Fernández, I. Bachiller, M. Barrio Luna, Cristina F. Bedoya, C.A. Carrillo Montoya, M. Cepeda, M. Cerrada, N. Colino, B. De La Cruz, A. Delgado Peris, J.P. Fernández Ramos, J. Flix, M.C. Fouz, O. Gonzalez Lopez, S. Goy Lopez, J.M. Hernandez, M.I. Josa, J. León Holgado, D. Moran, Á. Navarro Tobar, C. Perez Dengra, A. Pérez-Calero Yzquierdo, J. Puerta Pelayo, I. Redondo, L. Romero, S. Sánchez Navas, L. Urda Gómez, C. Willmott

Universidad Autónoma de Madrid, Madrid, Spain

J.F. de Trocóniz, R. Reyes-Almanza

Universidad de Oviedo, Instituto Universitario de Ciencias y Tecnologías Espaciales de Asturias (ICTEA), Oviedo, Spain

B. Alvarez Gonzalez, J. Cuevas, C. Erice, J. Fernandez Menendez, S. Folgueras, I. Gonzalez Caballero, J.R. González Fernández, E. Palencia Cortezon, C. Ramón Álvarez, V. Rodríguez Bouza, A. Trapote, N. Trevisani

Instituto de Física de Cantabria (IFCA), CSIC-Universidad de Cantabria, Santander, Spain

J.A. Brochero Cifuentes, I.J. Cabrillo, A. Calderon, J. Duarte Campderros, M. Fernandez, C. Fernandez Madrazo, P.J. Fernández Manteca, A. García Alonso, G. Gomez, C. Martinez Rivero, P. Martinez Ruiz del Arbol, F. Matorras, P. Matorras Cuevas, J. Piedra Gomez, C. Prieels, T. Rodrigo, A. Ruiz-Jimeno, L. Scodellaro, I. Vila, J.M. Vizan Garcia

University of Colombo, Colombo, Sri Lanka

MK Jayananda, B. Kailasapathy[59], D.U.J. Sonnadara, DDC Wickramarathna

University of Ruhuna, Department of Physics, Matara, Sri Lanka

W.G.D. Dharmaratna, K. Liyanage, N. Perera, N. Wickramage

CERN, European Organization for Nuclear Research, Geneva, Switzerland

T.K. Aarrestad, D. Abbaneo, J. Alimena, E. Auffray, G. Auzinger, J. Baechler, P. Baillon[†], D. Barney, J. Bendavid, M. Bianco, A. Bocci, T. Camporesi, M. Capeans Garrido, G. Cerminara, S.S. Chhibra, M. Cipriani, L. Cristella, D. d'Enterria, A. Dabrowski, N. Daci, A. David, A. De Roeck, M.M. Defranchis, M. Deile, M. Dobson, M. Dünser, N. Dupont, A. Elliott-Peisert, N. Emriskova, F. Fallavollita[60], D. Fasanella, A. Florent, G. Franzoni, W. Funk, S. Giani, D. Gigi, K. Gill, F. Glege, L. Gouskos, M. Haranko, J. Hegeman, Y. Iiyama, V. Innocente, T. James, P. Janot, J. Kaspar, J. Kieseler, M. Komm, N. Kratochwil, C. Lange, S. Laurila, P. Lecoq, K. Long, C. Lourenço, L. Malgeri, S. Mallios, M. Mannelli, A.C. Marini, F. Meijers, S. Mersi, E. Meschi, F. Moortgat, M. Mulders, S. Orfanelli, L. Orsini, F. Pantaleo, L. Pape, E. Perez, M. Peruzzi, A. Petrilli, G. Petrucciani, A. Pfeiffer, M. Pierini, D. Piparo, M. Pitt, H. Qu, T. Quast, D. Rabady, A. Racz, G. Reales Gutiérrez, M. Rieger, M. Rovere, H. Sakulin, J. Salfeld-Nebgen, S. Scarfi, C. Schäfer, C. Schwick, M. Selvaggi, A. Sharma, P. Silva, W. Snoeys, P. Sphicas[61], S. Summers, K. Tatar, V.R. Tavolaro, D. Treille, A. Tsirou, G.P. Van Onsem, M. Verzetti, J. Wanczyk[62], K.A. Wozniak, W.D. Zeuner

Paul Scherrer Institut, Villigen, Switzerland

L. Caminada[63], A. Ebrahimi, W. Erdmann, R. Horisberger, Q. Ingram, H.C. Kaestli, D. Kotlinski, U. Langenegger, M. Missiroli, T. Rohe

ETH Zurich - Institute for Particle Physics and Astrophysics (IPA), Zurich, Switzerland
K. Androsov[62], M. Backhaus, P. Berger, A. Calandri, N. Chernyavskaya, A. De Cosa, G. Dissertori, M. Dittmar, M. Donegà, C. Dorfer, F. Eble, K. Gedia, F. Glessgen, T.A. Gómez Espinosa, C. Grab, D. Hits, W. Lustermann, A.-M. Lyon, R.A. Manzoni, C. Martin Perez, M.T. Meinhard, F. Nessi-Tedaldi, J. Niedziela, F. Pauss, V. Perovic, S. Pigazzini, M.G. Ratti, M. Reichmann, C. Reissel, T. Reitenspiess, B. Ristic, D. Ruini, D.A. Sanz Becerra, M. Schönenberger, V. Stampf, J. Steggemann[62], R. Wallny, D.H. Zhu

Universität Zürich, Zurich, Switzerland
C. Amsler[64], P. Bärtschi, C. Botta, D. Brzhechko, M.F. Canelli, K. Cormier, A. De Wit, R. Del Burgo, J.K. Heikkilä, M. Huwiler, W. Jin, A. Jofrehei, B. Kilminster, S. Leontsinis, S.P. Liechti, A. Macchiolo, P. Meiring, V.M. Mikuni, U. Molinatti, I. Neutelings, A. Reimers, P. Robmann, S. Sanchez Cruz, K. Schweiger, Y. Takahashi

National Central University, Chung-Li, Taiwan
C. Adloff[65], C.M. Kuo, W. Lin, A. Roy, T. Sarkar[36], S.S. Yu

National Taiwan University (NTU), Taipei, Taiwan
L. Ceard, Y. Chao, K.F. Chen, P.H. Chen, W.-S. Hou, Y.y. Li, R.-S. Lu, E. Paganis, A. Psallidas, A. Steen, H.y. Wu, E. Yazgan, P.r. Yu

Chulalongkorn University, Faculty of Science, Department of Physics, Bangkok, Thailand
B. Asavapibhop, C. Asawatangtrakuldee, N. Srimanobhas

Çukurova University, Physics Department, Science and Art Faculty, Adana, Turkey
F. Boran, S. Damarseckin[66], Z.S. Demiroglu, F. Dolek, I. Dumanoglu[67], E. Eskut, Y. Guler, E. Gurpinar Guler[68], I. Hos[69], C. Isik, O. Kara, A. Kayis Topaksu, U. Kiminsu, G. Onengut, K. Ozdemir[70], A. Polatoz, A.E. Simsek, B. Tali[71], U.G. Tok, S. Turkcapar, I.S. Zorbakir, C. Zorbilmez

Middle East Technical University, Physics Department, Ankara, Turkey
B. Isildak[72], G. Karapinar[73], K. Ocalan[74], M. Yalvac[75]

Bogazici University, Istanbul, Turkey
B. Akgun, I.O. Atakisi, E. Gülmez, M. Kaya[76], O. Kaya[77], Ö. Özçelik, S. Tekten[78], E.A. Yetkin[79]

Istanbul Technical University, Istanbul, Turkey
A. Cakir, K. Cankocak[67], Y. Komurcu, S. Sen[80]

Istanbul University, Istanbul, Turkey
S. Cerci[71], B. Kaynak, S. Ozkorucuklu, D. Sunar Cerci[71]

Institute for Scintillation Materials of National Academy of Science of Ukraine, Kharkov, Ukraine
B. Grynyov

National Scientific Center, Kharkov Institute of Physics and Technology, Kharkov, Ukraine
L. Levchuk

University of Bristol, Bristol, United Kingdom
D. Anthony, E. Bhal, S. Bologna, J.J. Brooke, A. Bundock, E. Clement, D. Cussans, H. Flacher, J. Goldstein, G.P. Heath, H.F. Heath, M.l. Holmberg[81], L. Kreczko, B. Krikler, S. Paramesvaran, S. Seif El Nasr-Storey, V.J. Smith, N. Stylianou[82], K. Walkingshaw Pass, R. White

Rutherford Appleton Laboratory, Didcot, United Kingdom
K.W. Bell, A. Belyaev[83], C. Brew, R.M. Brown, D.J.A. Cockerill, C. Cooke, K.V. Ellis, K. Harder,

S. Harper, J. Linacre, K. Manolopoulos, D.M. Newbold, E. Olaiya, D. Petyt, T. Reis, T. Schuh, C.H. Shepherd-Themistocleous, I.R. Tomalin, T. Williams

Imperial College, London, United Kingdom
R. Bainbridge, P. Bloch, S. Bonomally, J. Borg, S. Breeze, O. Buchmuller, V. Cepaitis, G.S. Chahal[84], D. Colling, P. Dauncey, G. Davies, M. Della Negra, S. Fayer, G. Fedi, G. Hall, M.H. Hassanshahi, G. Iles, J. Langford, L. Lyons, A.-M. Magnan, S. Malik, A. Martelli, D.G. Monk, J. Nash[85], M. Pesaresi, D.M. Raymond, A. Richards, A. Rose, E. Scott, C. Seez, A. Shtipliyski, A. Tapper, K. Uchida, T. Virdee[20], M. Vojinovic, N. Wardle, S.N. Webb, D. Winterbottom, A.G. Zecchinelli

Brunel University, Uxbridge, United Kingdom
K. Coldham, J.E. Cole, A. Khan, P. Kyberd, I.D. Reid, L. Teodorescu, S. Zahid

Baylor University, Waco, USA
S. Abdullin, A. Brinkerhoff, B. Caraway, J. Dittmann, K. Hatakeyama, A.R. Kanuganti, B. McMaster, N. Pastika, M. Saunders, S. Sawant, C. Sutantawibul, J. Wilson

Catholic University of America, Washington, DC, USA
R. Bartek, A. Dominguez, R. Uniyal, A.M. Vargas Hernandez

The University of Alabama, Tuscaloosa, USA
A. Buccilli, S.I. Cooper, D. Di Croce, S.V. Gleyzer, C. Henderson, C.U. Perez, P. Rumerio[86], C. West

Boston University, Boston, USA
A. Akpinar, A. Albert, D. Arcaro, C. Cosby, Z. Demiragli, E. Fontanesi, D. Gastler, J. Rohlf, K. Salyer, D. Sperka, D. Spitzbart, I. Suarez, A. Tsatsos, S. Yuan, D. Zou

Brown University, Providence, USA
G. Benelli, B. Burkle, X. Coubez[21], D. Cutts, M. Hadley, U. Heintz, J.M. Hogan[87], G. Landsberg, K.T. Lau, M. Lukasik, J. Luo, M. Narain, S. Sagir[88], E. Usai, W.Y. Wong, X. Yan, D. Yu, W. Zhang

University of California, Davis, Davis, USA
J. Bonilla, C. Brainerd, R. Breedon, M. Calderon De La Barca Sanchez, M. Chertok, J. Conway, P.T. Cox, R. Erbacher, G. Haza, F. Jensen, O. Kukral, R. Lander, M. Mulhearn, D. Pellett, B. Regnery, D. Taylor, Y. Yao, F. Zhang

University of California, Los Angeles, USA
M. Bachtis, R. Cousins, A. Datta, D. Hamilton, J. Hauser, M. Ignatenko, M.A. Iqbal, T. Lam, W.A. Nash, S. Regnard, D. Saltzberg, B. Stone, V. Valuev

University of California, Riverside, Riverside, USA
K. Burt, Y. Chen, R. Clare, J.W. Gary, M. Gordon, G. Hanson, G. Karapostoli, O.R. Long, N. Manganelli, M. Olmedo Negrete, W. Si, S. Wimpenny, Y. Zhang

University of California, San Diego, La Jolla, USA
J.G. Branson, P. Chang, S. Cittolin, S. Cooperstein, N. Deelen, D. Diaz, J. Duarte, R. Gerosa, L. Giannini, D. Gilbert, J. Guiang, R. Kansal, V. Krutelyov, R. Lee, J. Letts, M. Masciovecchio, S. May, M. Pieri, B.V. Sathia Narayanan, V. Sharma, M. Tadel, A. Vartak, F. Würthwein, Y. Xiang, A. Yagil

University of California, Santa Barbara - Department of Physics, Santa Barbara, USA
N. Amin, C. Campagnari, M. Citron, A. Dorsett, V. Dutta, J. Incandela, M. Kilpatrick, J. Kim,

B. Marsh, H. Mei, M. Oshiro, M. Quinnan, J. Richman, U. Sarica, F. Setti, J. Sheplock, D. Stuart, S. Wang

California Institute of Technology, Pasadena, USA
A. Bornheim, O. Cerri, I. Dutta, J.M. Lawhorn, N. Lu, J. Mao, H.B. Newman, T.Q. Nguyen, M. Spiropulu, J.R. Vlimant, C. Wang, S. Xie, Z. Zhang, R.Y. Zhu

Carnegie Mellon University, Pittsburgh, USA
J. Alison, S. An, M.B. Andrews, P. Bryant, T. Ferguson, A. Harilal, C. Liu, T. Mudholkar, M. Paulini, A. Sanchez, W. Terrill

University of Colorado Boulder, Boulder, USA
J.P. Cumalat, W.T. Ford, A. Hassani, E. MacDonald, R. Patel, A. Perloff, C. Savard, K. Stenson, K.A. Ulmer, S.R. Wagner

Cornell University, Ithaca, USA
J. Alexander, S. Bright-thonney, Y. Cheng, D.J. Cranshaw, S. Hogan, J. Monroy, J.R. Patterson, D. Quach, J. Reichert, M. Reid, A. Ryd, W. Sun, J. Thom, P. Wittich, R. Zou

Fermi National Accelerator Laboratory, Batavia, USA
M. Albrow, M. Alyari, G. Apollinari, A. Apresyan, A. Apyan, S. Banerjee, L.A.T. Bauerdick, D. Berry, J. Berryhill, P.C. Bhat, K. Burkett, J.N. Butler, A. Canepa, G.B. Cerati, H.W.K. Cheung, F. Chlebana, M. Cremonesi, K.F. Di Petrillo, V.D. Elvira, Y. Feng, J. Freeman, Z. Gecse, L. Gray, D. Green, S. Grünendahl, O. Gutsche, R.M. Harris, R. Heller, T.C. Herwig, J. Hirschauer, B. Jayatilaka, S. Jindariani, M. Johnson, U. Joshi, T. Klijnsma, B. Klima, K.H.M. Kwok, S. Lammel, D. Lincoln, R. Lipton, T. Liu, C. Madrid, K. Maeshima, C. Mantilla, D. Mason, P. McBride, P. Merkel, S. Mrenna, S. Nahn, J. Ngadiuba, V. O'Dell, V. Papadimitriou, K. Pedro, C. Pena[56], O. Prokofyev, F. Ravera, A. Reinsvold Hall, L. Ristori, B. Schneider, E. Sexton-Kennedy, N. Smith, A. Soha, W.J. Spalding, L. Spiegel, S. Stoynev, J. Strait, L. Taylor, S. Tkaczyk, N.V. Tran, L. Uplegger, E.W. Vaandering, H.A. Weber

University of Florida, Gainesville, USA
D. Acosta, P. Avery, D. Bourilkov, L. Cadamuro, V. Cherepanov, F. Errico, R.D. Field, D. Guerrero, B.M. Joshi, M. Kim, E. Koenig, J. Konigsberg, A. Korytov, K.H. Lo, K. Matchev, N. Menendez, G. Mitselmakher, A. Muthirakalayil Madhu, N. Rawal, D. Rosenzweig, S. Rosenzweig, K. Shi, J. Sturdy, J. Wang, E. Yigitbasi, X. Zuo

Florida State University, Tallahassee, USA
T. Adams, A. Askew, R. Habibullah, V. Hagopian, K.F. Johnson, R. Khurana, T. Kolberg, G. Martinez, H. Prosper, C. Schiber, O. Viazlo, R. Yohay, J. Zhang

Florida Institute of Technology, Melbourne, USA
M.M. Baarmand, S. Butalla, T. Elkafrawy[89], M. Hohlmann, R. Kumar Verma, D. Noonan, M. Rahmani, F. Yumiceva

University of Illinois at Chicago (UIC), Chicago, USA
M.R. Adams, H. Becerril Gonzalez, R. Cavanaugh, X. Chen, S. Dittmer, O. Evdokimov, C.E. Gerber, D.A. Hangal, D.J. Hofman, A.H. Merrit, C. Mills, G. Oh, T. Roy, S. Rudrabhatla, M.B. Tonjes, N. Varelas, J. Viinikainen, X. Wang, Z. Wu, Z. Ye

The University of Iowa, Iowa City, USA
M. Alhusseini, K. Dilsiz[90], R.P. Gandrajula, O.K. Köseyan, J.-P. Merlo, A. Mestvirishvili[91], J. Nachtman, H. Ogul[92], Y. Onel, A. Penzo, C. Snyder, E. Tiras[93]

Johns Hopkins University, Baltimore, USA
O. Amram, B. Blumenfeld, L. Corcodilos, J. Davis, M. Eminizer, A.V. Gritsan, S. Kyriacou, P. Maksimovic, J. Roskes, M. Swartz, T.Á. Vámi

The University of Kansas, Lawrence, USA
A. Abreu, J. Anguiano, C. Baldenegro Barrera, P. Baringer, A. Bean, A. Bylinkin, Z. Flowers, T. Isidori, S. Khalil, J. King, G. Krintiras, A. Kropivnitskaya, M. Lazarovits, C. Lindsey, J. Marquez, N. Minafra, M. Murray, M. Nickel, C. Rogan, C. Royon, R. Salvatico, S. Sanders, E. Schmitz, C. Smith, J.D. Tapia Takaki, Q. Wang, Z. Warner, J. Williams, G. Wilson

Kansas State University, Manhattan, USA
S. Duric, A. Ivanov, K. Kaadze, D. Kim, Y. Maravin, T. Mitchell, A. Modak, K. Nam

Lawrence Livermore National Laboratory, Livermore, USA
F. Rebassoo, D. Wright

University of Maryland, College Park, USA
E. Adams, A. Baden, O. Baron, A. Belloni, S.C. Eno, N.J. Hadley, S. Jabeen, R.G. Kellogg, T. Koeth, A.C. Mignerey, S. Nabili, C. Palmer, M. Seidel, A. Skuja, L. Wang, K. Wong

Massachusetts Institute of Technology, Cambridge, USA
D. Abercrombie, G. Andreassi, R. Bi, S. Brandt, W. Busza, I.A. Cali, Y. Chen, M. D'Alfonso, J. Eysermans, C. Freer, G. Gomez Ceballos, M. Goncharov, P. Harris, M. Hu, M. Klute, D. Kovalskyi, J. Krupa, Y.-J. Lee, B. Maier, C. Mironov, C. Paus, D. Rankin, C. Roland, G. Roland, Z. Shi, G.S.F. Stephans, J. Wang, Z. Wang, B. Wyslouch

University of Minnesota, Minneapolis, USA
R.M. Chatterjee, A. Evans, P. Hansen, J. Hiltbrand, Sh. Jain, M. Krohn, Y. Kubota, J. Mans, M. Revering, R. Rusack, R. Saradhy, N. Schroeder, N. Strobbe, M.A. Wadud

University of Nebraska-Lincoln, Lincoln, USA
K. Bloom, M. Bryson, S. Chauhan, D.R. Claes, C. Fangmeier, L. Finco, F. Golf, C. Joo, I. Kravchenko, M. Musich, I. Reed, J.E. Siado, G.R. Snow[+], W. Tabb, F. Yan

State University of New York at Buffalo, Buffalo, USA
G. Agarwal, H. Bandyopadhyay, L. Hay, I. Iashvili, A. Kharchilava, C. McLean, D. Nguyen, J. Pekkanen, S. Rappoccio, A. Williams

Northeastern University, Boston, USA
G. Alverson, E. Barberis, Y. Haddad, A. Hortiangtham, J. Li, G. Madigan, B. Marzocchi, D.M. Morse, V. Nguyen, T. Orimoto, A. Parker, L. Skinnari, A. Tishelman-Charny, T. Wamorkar, B. Wang, A. Wisecarver, D. Wood

Northwestern University, Evanston, USA
S. Bhattacharya, J. Bueghly, Z. Chen, A. Gilbert, T. Gunter, K.A. Hahn, Y. Liu, N. Odell, M.H. Schmitt, M. Velasco

University of Notre Dame, Notre Dame, USA
R. Band, R. Bucci, A. Das, N. Dev, R. Goldouzian, M. Hildreth, K. Hurtado Anampa, C. Jessop, K. Lannon, J. Lawrence, N. Loukas, D. Lutton, N. Marinelli, I. Mcalister, T. McCauley, C. Mcgrady, F. Meng, K. Mohrman, Y. Musienko[49], R. Ruchti, P. Siddireddy, A. Townsend, M. Wayne, A. Wightman, M. Wolf, M. Zarucki, L. Zygala

The Ohio State University, Columbus, USA
B. Bylsma, B. Cardwell, L.S. Durkin, B. Francis, C. Hill, M. Nunez Ornelas, K. Wei, B.L. Winer, B.R. Yates

Princeton University, Princeton, USA
F.M. Addesa, B. Bonham, P. Das, G. Dezoort, P. Elmer, A. Frankenthal, B. Greenberg, N. Haubrich, S. Higginbotham, A. Kalogeropoulos, G. Kopp, S. Kwan, D. Lange, M.T. Lucchini, D. Marlow, K. Mei, I. Ojalvo, J. Olsen, D. Stickland, C. Tully

University of Puerto Rico, Mayaguez, USA
S. Malik, S. Norberg

Purdue University, West Lafayette, USA
A.S. Bakshi, V.E. Barnes, R. Chawla, S. Das, L. Gutay, M. Jones, A.W. Jung, S. Karmarkar, M. Liu, G. Negro, N. Neumeister, G. Paspalaki, C.C. Peng, S. Piperov, A. Purohit, J.F. Schulte, M. Stojanovic[16], J. Thieman, F. Wang, R. Xiao, W. Xie

Purdue University Northwest, Hammond, USA
J. Dolen, N. Parashar

Rice University, Houston, USA
A. Baty, M. Decaro, S. Dildick, K.M. Ecklund, S. Freed, P. Gardner, F.J.M. Geurts, A. Kumar, W. Li, B.P. Padley, R. Redjimi, W. Shi, A.G. Stahl Leiton, S. Yang, L. Zhang, Y. Zhang

University of Rochester, Rochester, USA
A. Bodek, P. de Barbaro, R. Demina, J.L. Dulemba, C. Fallon, T. Ferbel, M. Galanti, A. Garcia-Bellido, O. Hindrichs, A. Khukhunaishvili, E. Ranken, R. Taus

Rutgers, The State University of New Jersey, Piscataway, USA
B. Chiarito, J.P. Chou, A. Gandrakota, Y. Gershtein, E. Halkiadakis, A. Hart, M. Heindl, O. Karacheban[24], I. Laflotte, A. Lath, R. Montalvo, K. Nash, M. Osherson, S. Salur, S. Schnetzer, S. Somalwar, R. Stone, S.A. Thayil, S. Thomas, H. Wang

University of Tennessee, Knoxville, USA
H. Acharya, A.G. Delannoy, S. Fiorendi, S. Spanier

Texas A&M University, College Station, USA
O. Bouhali[94], M. Dalchenko, A. Delgado, R. Eusebi, J. Gilmore, T. Huang, T. Kamon[95], H. Kim, S. Luo, S. Malhotra, R. Mueller, D. Overton, D. Rathjens, A. Safonov

Texas Tech University, Lubbock, USA
N. Akchurin, J. Damgov, V. Hegde, S. Kunori, K. Lamichhane, S.W. Lee, T. Mengke, S. Muthumuni, T. Peltola, I. Volobouev, Z. Wang, A. Whitbeck

Vanderbilt University, Nashville, USA
E. Appelt, S. Greene, A. Gurrola, W. Johns, A. Melo, H. Ni, K. Padeken, F. Romeo, P. Sheldon, S. Tuo, J. Velkovska

University of Virginia, Charlottesville, USA
M.W. Arenton, B. Cox, G. Cummings, J. Hakala, R. Hirosky, M. Joyce, A. Ledovskoy, A. Li, C. Neu, B. Tannenwald, S. White, E. Wolfe

Wayne State University, Detroit, USA
R. Harr, N. Poudyal

University of Wisconsin - Madison, Madison, WI, USA

K. Black, T. Bose, C. Caillol, S. Dasu, I. De Bruyn, P. Everaerts, F. Fienga, C. Galloni, H. He, M. Herndon, A. Hervé, U. Hussain, A. Lanaro, A. Loeliger, R. Loveless, J. Madhusudanan Sreekala, A. Mallampalli, A. Mohammadi, D. Pinna, A. Savin, V. Shang, V. Sharma, W.H. Smith, D. Teague, S. Trembath-reichert, W. Vetens

†: Deceased
1: Also at TU Wien, Wien, Austria
2: Also at Institute of Basic and Applied Sciences, Faculty of Engineering, Arab Academy for Science, Technology and Maritime Transport, Alexandria, Egypt, Alexandria, Egypt
3: Also at Université Libre de Bruxelles, Bruxelles, Belgium
4: Also at Universidade Estadual de Campinas, Campinas, Brazil
5: Also at Federal University of Rio Grande do Sul, Porto Alegre, Brazil
6: Also at University of Chinese Academy of Sciences, Beijing, China
7: Also at Department of Physics, Tsinghua University, Beijing, China, Beijing, China
8: Also at UFMS, Nova Andradina, Brazil
9: Also at Nanjing Normal University Department of Physics, Nanjing, China
10: Now at The University of Iowa, Iowa City, USA
11: Also at Institute for Theoretical and Experimental Physics named by A.I. Alikhanov of NRC 'Kurchatov Institute', Moscow, Russia
12: Also at Joint Institute for Nuclear Research, Dubna, Russia
13: Also at Helwan University, Cairo, Egypt
14: Now at Zewail City of Science and Technology, Zewail, Egypt
15: Now at Cairo University, Cairo, Egypt
16: Also at Purdue University, West Lafayette, USA
17: Also at Université de Haute Alsace, Mulhouse, France
18: Also at Tbilisi State University, Tbilisi, Georgia
19: Also at Erzincan Binali Yildirim University, Erzincan, Turkey
20: Also at CERN, European Organization for Nuclear Research, Geneva, Switzerland
21: Also at RWTH Aachen University, III. Physikalisches Institut A, Aachen, Germany
22: Also at University of Hamburg, Hamburg, Germany
23: Also at Department of Physics, Isfahan University of Technology, Isfahan, Iran, Isfahan, Iran
24: Also at Brandenburg University of Technology, Cottbus, Germany
25: Also at Physics Department, Faculty of Science, Assiut University, Assiut, Egypt
26: Also at Karoly Robert Campus, MATE Institute of Technology, Gyongyos, Hungary
27: Also at Institute of Physics, University of Debrecen, Debrecen, Hungary, Debrecen, Hungary
28: Also at Institute of Nuclear Research ATOMKI, Debrecen, Hungary
29: Also at MTA-ELTE Lendület CMS Particle and Nuclear Physics Group, Eötvös Loránd University, Budapest, Hungary, Budapest, Hungary
30: Also at Wigner Research Centre for Physics, Budapest, Hungary
31: Also at IIT Bhubaneswar, Bhubaneswar, India, Bhubaneswar, India
32: Also at Institute of Physics, Bhubaneswar, India
33: Also at G.H.G. Khalsa College, Punjab, India
34: Also at Shoolini University, Solan, India
35: Also at University of Hyderabad, Hyderabad, India
36: Also at University of Visva-Bharati, Santiniketan, India
37: Also at Indian Institute of Technology (IIT), Mumbai, India
38: Also at Deutsches Elektronen-Synchrotron, Hamburg, Germany

39: Also at Sharif University of Technology, Tehran, Iran

40: Also at Department of Physics, University of Science and Technology of Mazandaran, Behshahr, Iran

41: Now at INFN Sezione di Bari ^{a}, Università di Bari ^{b}, Politecnico di Bari ^{c}, Bari, Italy

42: Also at Italian National Agency for New Technologies, Energy and Sustainable Economic Development, Bologna, Italy

43: Also at Centro Siciliano di Fisica Nucleare e di Struttura Della Materia, Catania, Italy

44: Also at Università di Napoli 'Federico II', NAPOLI, Italy

45: Also at Consiglio Nazionale delle Ricerche - Istituto Officina dei Materiali, PERUGIA, Italy

46: Also at Riga Technical University, Riga, Latvia, Riga, Latvia

47: Also at Consejo Nacional de Ciencia y Tecnología, Mexico City, Mexico

48: Also at IRFU, CEA, Université Paris-Saclay, Gif-sur-Yvette, France

49: Also at Institute for Nuclear Research, Moscow, Russia

50: Now at National Research Nuclear University 'Moscow Engineering Physics Institute' (MEPhI), Moscow, Russia

51: Also at Institute of Nuclear Physics of the Uzbekistan Academy of Sciences, Tashkent, Uzbekistan

52: Also at St. Petersburg State Polytechnical University, St. Petersburg, Russia

53: Also at University of Florida, Gainesville, USA

54: Also at Imperial College, London, United Kingdom

55: Also at P.N. Lebedev Physical Institute, Moscow, Russia

56: Also at California Institute of Technology, Pasadena, USA

57: Also at Budker Institute of Nuclear Physics, Novosibirsk, Russia

58: Also at Faculty of Physics, University of Belgrade, Belgrade, Serbia

59: Also at Trincomalee Campus, Eastern University, Sri Lanka, Nilaveli, Sri Lanka

60: Also at INFN Sezione di Pavia ^{a}, Università di Pavia ^{b}, Pavia, Italy, Pavia, Italy

61: Also at National and Kapodistrian University of Athens, Athens, Greece

62: Also at Ecole Polytechnique Fédérale Lausanne, Lausanne, Switzerland

63: Also at Universität Zürich, Zurich, Switzerland

64: Also at Stefan Meyer Institute for Subatomic Physics, Vienna, Austria, Vienna, Austria

65: Also at Laboratoire d'Annecy-le-Vieux de Physique des Particules, IN2P3-CNRS, Annecy-le-Vieux, France

66: Also at Şırnak University, Sirnak, Turkey

67: Also at Near East University, Research Center of Experimental Health Science, Nicosia, Turkey

68: Also at Konya Technical University, Konya, Turkey

69: Also at Istanbul University - Cerrahpasa, Faculty of Engineering, Istanbul, Turkey

70: Also at Piri Reis University, Istanbul, Turkey

71: Also at Adiyaman University, Adiyaman, Turkey

72: Also at Ozyegin University, Istanbul, Turkey

73: Also at Izmir Institute of Technology, Izmir, Turkey

74: Also at Necmettin Erbakan University, Konya, Turkey

75: Also at Bozok Universitetesi Rektörlügü, Yozgat, Turkey, Yozgat, Turkey

76: Also at Marmara University, Istanbul, Turkey

77: Also at Milli Savunma University, Istanbul, Turkey

78: Also at Kafkas University, Kars, Turkey

79: Also at Istanbul Bilgi University, Istanbul, Turkey

80: Also at Hacettepe University, Ankara, Turkey

81: Also at Rutherford Appleton Laboratory, Didcot, United Kingdom

82: Also at Vrije Universiteit Brussel, Brussel, Belgium

83: Also at School of Physics and Astronomy, University of Southampton, Southampton, United Kingdom

84: Also at IPPP Durham University, Durham, United Kingdom

85: Also at Monash University, Faculty of Science, Clayton, Australia

86: Also at Università di Torino, TORINO, Italy

87: Also at Bethel University, St. Paul, Minneapolis, USA, St. Paul, USA

88: Also at Karamanoğlu Mehmetbey University, Karaman, Turkey

89: Also at Ain Shams University, Cairo, Egypt

90: Also at Bingol University, Bingol, Turkey

91: Also at Georgian Technical University, Tbilisi, Georgia

92: Also at Sinop University, Sinop, Turkey

93: Also at Erciyes University, KAYSERI, Turkey

94: Also at Texas A&M University at Qatar, Doha, Qatar

95: Also at Kyungpook National University, Daegu, Korea, Daegu, Korea